Trypanosome morphogenesis involves recruitment of a pleckstrin homology domain protein by an orphan kinesin to the microtubule quartet

Corinna Benz[1], Nora Müller[2], Marie Vancová[1,2], Sabine Kaltenbrunner[1,2,†], Hana Váchová[3], Vladimír Varga[3], Julius Lukeš[1,2], Hassan Hashimi[1,2,*]

[1]Institute of Parasitology, Biology Center, Czech Academy of Sciences, České Budějovice, Czechia

[2] Faculty of Science, University of South Bohemia, České Budějovice, Czechia

[3]Laboratory of Cell Motility, Institute of Molecular Genetics of the Czech Academy of Sciences, Prague, Czechia

[†]Current address: Johannes Kepler University, Medical Faculty, Linz, Austria

*Corresponding author: hassan@paru.cas.cz

Running title: TbKifX2 and TbPH1 associate with the trypanosomal microtubule quartet

ABSTRACT

Kinesins are motor proteins found in all eukaryotic lineages that move along microtubule tracks to mediate numerous cellular processes such as mitosis and intracellular transport of cargo. In

trypanosomatids, the kinesin protein superfamily has undergone a prominent expansion, giving these protists one of the most diverse kinesin repertoires. This has led to the emergence of two trypanosomatid-restricted groups of kinesins. Here, we characterize in *Trypanosoma brucei* TbKifX2, a hitherto orphaned kinesin that belongs to one of these groups. TbKifX2 tightly interacts with TbPH1, a kinesin-like protein named after a pleckstrin homology (PH) domain present within its carboxy terminal tail. TbKifX2 recruits TbPH1 to the microtubule quartet (MtQ), a characteristic cytoskeletal structure that is part of the multipartite flagellum attachment zone (FAZ) and extends from the basal body to the anterior of the cell body. The proximal proteome of TbPH1 is comprised of four proteins that localize to the FAZ, consistent with the notion that the TbKifX2/TbPH1 complex binds the MtQ along its whole length. Simultaneous ablation of both TbKifX2 and TbPH1 leads to the formation of prominent protrusions from the cell posterior. Thus, we have attributed a morphogenesis role to these two trypanosomatid-restricted proteins, and their remarkably specific localization to the MtQ in a microtubule-rich cell. We hypothesize that the putative TbKifX2/TbPH1 complex transports a cytokinesis auxiliary factor(s) along the MtQ to or from the *T. brucei* posterior. The cohort of proteins found in proximity to TbPH1 may represent one of these factors directly or be involved in their trafficking during cell division in trypanosomatids.

AUTHOR SUMMARY

Trypanosomatids are a group of unicellular parasites that infect a wide range of hosts from land plants to animals. They are also eukaryotes that have been shaped by prolonged independent evolution since this domain of life has radiated from a common ancestor almost 2 billion years ago. Thus, any resulting unique biological properties can be potentially exploited for treatment of infectious diseases caused by trypanosomatids. The cytoskeleton of trypanosomatids represents an ancient organelle that has undergone such modification. Here, we show that two trypanosomatid-

specific proteins named TbPH1 and TbKifX2 form a complex that localizes to the microtubule quartet, a cytoskeletal structure characteristic to trypanosomatids. Ablation of these proteins in *Trypansoma brucei* leads to severe morphological defects, making them not only intrinsically interesting topics of study, but potential therapeutic targets as well.

INTRODUCTION

The vermiform morphology of the unicellular parasite *Trypanosoma brucei* that causes African trypanosomiasis in humans and nagana in cattle is defined by a subpellicular array of microtubules (MTs) [1–3]. These MTs follow the helical path of the cell and are cross-linked to each other and the plasma membrane via regularly spaced fibrils [4]. A high order is maintained within the corset with the MT plus ends converging at the parasite's posterior end and the minus ends located at the anterior of the cell [3].

The only place where the continuity of the *T. brucei* MT array is interrupted is at the flagellar pocket, the deep invagination where the flagellum exits the cell body and the only place where endo- and exocytoses occur [5]. The opening of the flagellar pocket is encircled by a collar, which influences the overall shape of this cavity. Distal to the collar, the so-called hook complex covers the flagellum as it exits the flagellar pocket, with two lateral arms also flanking the flagellum attachment zone (FAZ) filament and the MT quartet (MtQ) inside the cell [6]. The FAZ filament and MtQ are among the interconnected fibres, filaments and junctional complexes of the multipartite FAZ [7], which together form a lateral attachment for the flagellum as it follows a helical path along the cell body, connecting the flagellar skeleton to the cytoskeleton through both the flagellar and plasma membranes [8]. The MtQ originates close to the basal bodies, wraps itself around the flagellar pocket and interdigitates within the MT corset next to the FAZ filament. The orientation of MTs in the MtQ is antiparallel to the one found within the MT corset, thus their minus ends are proximal to the basal bodies [3].

70 The trypanosome MT corset is exceptionally stable and only reorganised during cell division and life
71 cycle transitions [9]. All cytoskeletal structures (MtQ, MT corset, flagellum, basal bodies, which
72 anchor the flagella within the cell, and FAZ) need to be duplicated and faithfully segregated during
73 the cell division cycle, just like other single-copy organelles. In addition, this has to be coordinated
74 with replication and division of the nucleus and the single mitochondrial DNA network termed the
75 kinetoplast, which is located on the opposite side of the basal bodies relative to the flagellum [3,10].

76 Basal body duplication and segregation are the first visible steps in the cell division cycle and
77 essential for subsequent cytokinesis [11]. The new MtQ starts growing just prior to basal body
78 maturation and once the new flagellum has grown enough to invade the flagellar pocket,
79 morphogenetic changes result in two separate pockets enveloping both the new and old flagella
80 [12]. New corset MTs are nucleated from the side of the existing ones and elongate on both the plus
81 and minus ends during array replication [4]. Once the new flagellum has been nucleated and
82 elongated, new MTs are integrated into the array between the old and new flagella, thereby
83 increasing the overall width of the cell [1].

84 With its antiparallel orientation, the MtQ together with the FAZ filament create an asymmetric seam
85 within the MT corset, which works as a cellular ruler and helps to determine the site of future furrow
86 ingression during cytokinesis [8]. Any insults to the integrity of these structures result in cytokinesis
87 defects and it is thus tempting to envision the MtQ as a potential specialised “highway” in charge of
88 transport and delivery of cargo to the site of important cytokinesis events. Furthermore, the
89 endplasmic reticulum associates with parts of the MtQ, although the upshot of this association
90 remains mysterious. The first protein localized to this structure, TbSpef1, is found at the proximal
91 end of the MtQ, between basal bodies and the flagellar pocket collar [13]. Its depletion causes
92 problems with the biogenesis of the MtQ and associated structures as well as motility defects. The
93 minus end of the MtQ MTs is anchored to the basal bodies by a protein named TbSAF1, found in
94 close proximity to TbSpef1 but localized between the pro and mature basal bodies [14]. TbSAF1 was

95 found in a proximal proteomics screen of proteins adjoining to and/or directly interacting with
96 TbSpef1 (*i.e.* the TbSpef1 proxisome), which found three additional proteins that localize to the MtQ
97 between the basal body and flagellar pocket collar [14]. However, no proteins that localise along the
98 total length of the MtQ have thus far been identified nor have any motor proteins that may
99 potentially bring cargo to the cytokinesis site.

100 Kinesins are well-studied motor proteins that regulate MT dynamics, organize MT networks, and
101 transport cargo along MTs. Transporting kinesins can form homo- and heterodimers and consist of a
102 head region containing the kinesin motor domain, which is responsible for ATP hydrolysis and MT
103 binding, and a tail region important for dimerization with a kinesin/kinesin-like partner and cargo
104 binding [15]. In trypanosomatid genomes, kinesins and kinesin-like proteins constitute one of the
105 largest protein superfamilies [16–18]. To date, 47 genes encoding high-likelihood kinesins have been
106 identified in the *T. brucei* genome [19,20]. Moreover, there is a similar number of kinesin-related
107 proteins, which did not make the threshold due to sequence variance [16]. Interestingly, numerous
108 kinesins are members of two major clades named X-1 and X-2 that are restricted to the
109 trypanosomatid lineage [19,20]. Why the kinesin repertoire has expanded so prominently in
110 trypanosomatids remains mysterious.

111 Hitherto studied kinesins of *T. brucei* have been shown to be important for various processes
112 occurring in different cellular compartments. KinA and KinB are involved in cell cycle progression and
113 localise to the central spindle during mitosis [21] while TbKif13-1 localizes either to the nucleus or
114 the mitotic spindle, where it meditates chromosome segregation during mitosis [22]. KinC and KinD
115 are distributed throughout the cytoskeleton, where they are involved in subpellicular MT
116 organization, basal body segregation and cytokinesis [23,24].

117 Some kinesins are associated with the flagellum and adjacent FAZ. KIN2A and KIN2B are kinesins
118 involved in intraflagellar transport (IFT), a process that directly affects flagellar biogenesis and in turn
119 affects cell motility and cytokinesis [25,26]. The orphan kinesin KIN-E predominantly localises to the

120 flagellar tip and is required for elongation of the new FAZ [27]. Another orphan kinesin named KLIF
121 initially localises to the tip of the new, elongating FAZ and associates with the old FAZ as the
122 cytokinetic furrow ingresses towards the posterior end, thus mediating the final stages of cytokinesis
123 [28]. Other kinesins localising to specific cytoskeletal structures include FCP2/TbKinX1 and
124 FCP4/TbKin15, which are found at the flagella connector (FC), a trypanosome-specific structure that
125 connects the outgrowing new flagellum to the old one [29]. Interestingly, FCP2/TbKinX1 belongs to
126 kinesin clade X-1, one of the two trypanosomatid-restricted kinesin families [19,20].

127 Here we present data on the localisation and function of two members of the kinesin superfamily,
128 TbKifX2 and TbPH1, with the former protein belonging to clade X-2. Functional characterization and
129 the unique localization of these kinesins further expands our knowledge on how these diverse and
130 dexterous proteins affect biology of these extremely diverse and successful parasites.

131

132 **RESULTS**

133 **TbPH1 is a kinesin-like protein that fractionates with the *T. brucei* cytoskeleton**

134 TbPH1 (Tb927.3.2490) is a 110 kDa protein named after a C-terminal pleckstrin homology (PH)
135 domain, which is followed by a proximate homeodomain-like (HDL) fold and preceded by a coiled
136 coil (CC) domain (Fig. 1). The protein undergoes post-translational modifications, with
137 phosphorylation of a serine at the start of the HDL [30] and a methylarginine in the middle of the
138 primary structure [31]. While TbPH1 has an N-terminal kinesin motor domain, two substitutions of
139 highly conserved amino acids within the Walker A motif (G93P and T/S95R) likely ablate the ATP
140 hydrolase activity. Thus, TbPH1 is unlikely to be a *bona fide* kinesin motor protein**.**

141 TbPH1 also belongs to the ~2000 proteins found in the granule-enriched fraction (containing cellular
142 aggregates, nuclei, kinetoplasts and flagella as well as associated cytoskeletal structures) obtained
143 by 'MT sieving', a method originally conceived to purify stress granules from *T. brucei* [32]. In brief

144 (see S1 Fig. for 'MT sieving' pipeline), cells are lysed by non-ionic detergent in low ionic strength
145 buffer, which maintains the cytoskeleton, including the MT corset that in turn cages predominantly
146 detergent insoluble cellular structures with at least one dimension >20-30 nm. The cytoskeleton is
147 then disrupted by 300 mM NaCl to release these elements for subsequent analysis.

148 To verify TbPH1's apparent association with cytoskeletal fractions, we subjected a *T. brucei* cell line
149 in which the endogenous *TbPH1* open reading frame was appended with a C-terminal V5 tag [33] to
150 cell fractionation by a procedure identical to 'MT sieving'. The cell equivalents of the ensuing
151 fractions were inspected for the presence of TbPH1-V5 and SCD6, a stress granule marker that
152 served as a control for this method (Fig. 2A). SCD6 was mostly found in the soluble fractions as
153 previously reported for unstressed *T. brucei* [32], with a distribution across the analysed fractions
154 very distinct from that of TbPH1-V5. TbPH1-V5 was well retained in all cytoskeletal fractions P1 and
155 P2, although a fraction was released in the SN1 with other soluble cytosolic proteins upon initial lysis
156 (Fig. 2A). Importantly, indirect immunofluorescence (IFA) using an anti-V5 antibody on
157 formaldehyde-fixed P2 fraction shows that TbPH1-V5 is localized as a line extending from the DAPI-
158 stained kinetoplast (Fig. 2B) that decreases in signal intensity distally, suggestive of a cytoskeletal
159 localization. This was confirmed by the observation that the vast majority of TbPH1 was released
160 into the soluble SN3 fraction after high salt disintegration of the cytoskeleton. A small amount of
161 TbPH1-V5 was still found in the final pellet P3, which is consistent with its detection in the cohort of
162 proteins retained by 'MT sieving' [32]. Thus, TbPH1 is a kinesin-like protein that fractionates with the
163 trypanosomal cytoskeleton.

164

165 **TbPH1 strongly interacts with the trypanosomatid-restricted orphan kinesin TbKifX2**

166 Because kinesins tend to form dimers [34] and kinesin-like TbPH1 contains a CC domain (Fig. 1),
167 which usually mediates protein-protein interactions [35], we proceeded to see if TbPH1-V5 has an
168 interaction partner by immunoprecipitation (IP) via its C-terminal epitope tag. To enrich for soluble

169 TbPH1-V5 and augment IP stringency, we followed the previously described fractionation technique
170 above and used fraction SN3 as the input (Fig. 3A). A mock IP control using the parental cell line
171 without an expressed V5 epitope was performed in parallel.

172 After confirming immunocapture of TbPH1-V5 in the first eluate (Fig. 3A), the IP eluate from this and
173 the mock control were resolved on an SDS-PAGE gel. Sypro Ruby staining showed two prominent
174 bands of ~117 kDa (Fig. 3B, B1), the expected size for TbPH1-V5, and of ~80 kDa (Fig. 3B, B2).
175 Importantly, these bands were not observed in the mock control, indicating their presence is not due
176 to unspecific binding to the magnetic beads used to immobilize the anti-V5 antibody. Mass
177 spectrometry analysis of these two bands identified TbPH1 itself as expected and a previously
178 uncharacterised kinetoplastid-specific kinesin (Tb927.9.14750) (S1 Dataset), which we call TbKifX2
179 based on a previously proposed kinesin nomenclature [19]. In contrast to TbPH1, TbKifX2's kinesin
180 motor domain contains a conventional Walker A motif. This motor domain is located on the N-
181 terminus, indicating that TbKiFX2 most likely actively moves toward the plus-end of microtubules
182 [36]. It also contains a CC domain and two serine phosphorylation sites [30], similarly to TbPH1 (Fig.
183 1).

184 Interaction between these two proteins was further verified by tagging TbKifX2 with a C-terminal HA
185 tag in the TbPH1-V5 cell line. Indeed, TbKifX2 mirrored the fractionation pattern of TbPH1-V5 (Fig.
186 3C). As before, the SN3 fraction was used as an input for TbKifX2-HA IP, which co-
187 immunoprecipitated TbPH1-V5. Thus, we verified that TbPH1 and TbKifX2 exhibit a strong
188 interaction that persists even in 300 mM NaCl.

189 Whole cells expressing TbPH1-V5 and TbKifX2-HA were fixed and permeabilized prior to incubation
190 with antibodies recognizing either epitope-tag (Fig. 3D). We observed that both proteins possess a
191 considerable cell body signal that appears to be nucleus-excluded, with a prominent hook-like signal
192 along the proximal region of the flagellum. This pattern is consistent with the TrypTag localization
193 data, which visualized mNeonGreen-tagged proteins in immobilized live cells [37]. The cell body

194 signal likely represents the cytosolic population of both proteins that was also observed in our
195 fractionation data (Figs. 2A and 3C).

196

197 **Proximity proteomics reveals the spatial organization and interactors of TbPH1 and TbKifX2**

198 Since conventional IP of TbPH1-V5 under high salt conditions identified only TbKifX2 as its major
199 interaction partner, we sought a different method to identify potential cargo and/or interactors of
200 this putative kinesin complex. To do this, we tagged TbPH1 with a C-terminal biotin ligase 'BioID2'
201 [38], appended with an HA tag [39], to facilitate proximity-dependent biotin identification (BioID) of
202 neighbouring proteins. First, we determined by IFA on permeabilized whole cells using anti-HA
203 antibody that TbPH1-BioID2-HA localizes adjacent to the kinetoplast, which was also observed for
204 TbPH1-V5 (Figs. 2B and 4A). TbPH1-BioID2-HA also exhibited biotinylation activity in this part of the
205 cell, as visualized by streptavidin-conjugated to Alexa Fluor 488 (Fig. 4B). Thus, we confirmed that
206 the chimeric protein is properly localized and appears to biotinylate TbPH1 itself or proximal
207 proteins.

208 Purification of biotinylated proteins was performed as described elsewhere [40] (S2 Fig.). Western
209 blotting revealed that the vast majority of TbPH1-BioID2-HA was present in the soluble S1 fraction
210 (Fig. 4C), which was used for subsequent analysis. At first glance, this result appears to disagree with
211 previous findings from the 'MT sieving' fractionation, which employs comparable amounts of non-
212 ionic detergent and buffers of low ionic strength; however, we should emphasise that 'MT sieving'
213 fractionation uses a different detergent for a shorter incubation time and at a lower temperature in
214 comparison to the BioID purification (see Methods), which likely explains this difference.

215 Next, the S1 fraction was incubated with streptavidin-coated magnetic beads to capture biotinylated
216 proteins, which were subsequently trypsinized on beads prior to liquid chromatography-tandem
217 mass spectroscopy (LC-MS/MS). A mock control using the parental cell line lacking BioID2 expression

218 was processed in parallel. A total of 1,131 proteins were detected with high confidence (Andromeda
219 Protein Score ≥20; >1 unique peptide per protein) (S2 dataset). Following imputation of missing
220 values, seven proteins were shown to be preferentially biotinylated by TbPH1-BioID2-HA, as
221 visualised by plotting the -10 log t-test p value versus the t test difference in a volcano plot (Fig. 4D).
222 Statistically significant hits are found above the cut-off curve in this plot.

223 TbKifX2 was the most enriched protein based on both parameters, consistent with its strong
224 interaction with TbPH1. As expected, TbPH1 is also among the enriched proteins, indicating that
225 TbPH1-BioID2-HA biotinylated itself and/or a nearby untagged, endogenous form of the kinesin-like
226 protein. The sub-cellular location of the five novel proteins was determined using the TrypTag
227 protein localization resource [37]. This allowed us to already exclude one of them (Tb927.10.12110)
228 as a contaminant, given its nuclear localization. A putative kinesin with a C-terminal PH domain
229 (Tb927.6.2880) is enriched in the basal body. Two proteins are enriched in the flagellar pocket: a
230 dynamin-like protein 1/2 (DLP2, Tb927.3.4760; DLP1, Tb927.3.4720) and a flagellar pocket protein
231 FP45 (Tb927.9.9730). DLP1/2 is involved in clathrin-mediated endocytosis [41,42] as well as in
232 mitochondrial scission [41,43]**.** Interestingly, FP45 has also been demonstrated to be a soluble
233 protein that associates with the membrane surrounding the flagellar pocket by immunogold
234 labelling in an independent study [13]. Furthermore, TrypTag localization of FP45 often
235 demonstrates a line emanating from the flagellar pocket toward the anterior of the cell, similar to Tb
236 KifX2 and TbPH1. Only a putative flavin-trafficking protein (Tb927.8.1950) does not have a TrypTag
237 localization entry at this time. However, this protein was found among those that interact with
238 TOEFAZ1, a protein that associates with the tip of the extending FAZ (Fig. 4E) [28]. Furthermore,
239 Hilton and colleagues N-terminally tagged Tb927.8.1950 to determine its localization by IFA, which
240 exhibited an enriched signal in the vicinity of the kinetoplast.

241 These observations confirm the tight interaction between TbPH1 and TbKifX2. They also suggest that
242 these proteins associate with the basal body, a cytoskeletal element near the flagellar pocket, as

243 well as the FAZ given the localization of the biotinylated proteins. Indeed, both TbPH1 and TbKifX2
244 were also found within the TOEFAZ1-BioID proxisome with high statistical significance (P=0.001138
245 and 0.0032861, respectively), along with DLP1/2 (P=0.029631) (Fig. 4E) [28]. Furthermore, among
246 the most enriched proteins that were biotinylated by TbPH1-BioID2-HA, but just below the statistical
247 significance threshold, was a kinesin (Tb927.8.6830) that was found: 1) in the distal part of the FAZ
248 according to the TrypTag project; 2) within the TOEFAZ1 interactome with very high confidence
249 ($P=9.8 \times 10^{-6}$). Thus, we proceeded to test the basal body and FAZ localization suggested by the
250 TbPH1-BioID (Fig. 4) and IFA (Fig. 2A, 3D) results.

251

252 **TbPH1 and TbKifX2 localize to the microtubule quartet within the cytoskeleton**

253 We next decided to address whether TbPH1 and TbKifX2 localize to or near the FAZ, as was
254 suggested by the TbPH1 proxisome. Cytoskeletons were detergent-extracted from the TbPH1-V5 and
255 TbKifX-2 expressing cells to visualize any potential localization to discrete cytoskeletal structures.
256 Indeed both proteins co-localized to a long structure running along the long-axis of the cytoskeleton
257 adjacent to the flagellum (Fig. 5A). Furthermore, detergent extraction solubilized the cell body signal
258 (Fig. 3D), confirming it represented the cytosolic population of TbPH1 and TbKifX2 (Figs 2A and 3C).

259 We proceeded to identify specifically which cytoskeletal element TbPH1 and TbKifX2 associate with.
260 We used antibody recognizing TbKifX2-HA as a proxy for the TbKifX2-TbPH1 complex because of
261 their demonstrated tight interaction (Fig 3), and their co-localization on detergent-extracted
262 cytoskeletons (Fig. 5A). We found TbKifX2-HA to be juxtaposed with the FAZ filament, although the
263 former extended further toward the proximal region of the flagellum (Fig. 5B). This was confirmed
264 by TbKifX2-HA's co-localization with the basal bodies (Figs. 5C). This pattern led us to investigate
265 whether the kinesin was bound to the MtQ, as it originates close to the basal body and is considered
266 a part of the FAZ [7,8]. Indeed, TbKifX2 shows co-localization with a monoclonal antibody 1B41
267 recognizing the MtQ [44] (Fig. 5D).

268 To verify that TbKifX2 indeed binds the MtQ, we employed expansion microscopy (ExM) that
269 enlarges cells by embedding them within a swellable polyacrylamide matrix prior to immunolabelling
270 to allow examination of cellular structures in greater detail [45], and has recently been implemented
271 in *T. brucei* [46,47]. Performing ExM on the TbPH1-V5 and TbKifX2-HA-expressing cell line we
272 observed a punctate signal of an anti-V5 or anti-HA antibody in the cell body (Fig. 5E), consistent
273 with the significant cytosolic fraction of both proteins (Figs. 2A, 3C-D). Moreover, in some cells
274 localization of TbPH1-V5 or TbKifX2-HA to the part of the MtQ, which spirals around the flagellar
275 pocket, was apparent (Fig. 5F); this part of the MtQ is prominent in these ExM preparations [47]. The
276 associated V5 or HA signal was not discernible beyond the point of the MtQ joining the corset MTs,
277 where the signal of FAZ constituents, such as ClpGM6 [48], starts (S3 Fig.).The fact, that the signal of
278 TbPH1-V5 or TbKifX2-HA was apparent only in the part of the MtQ around the flagellar pocket is
279 consistent with this being the region of the highest concentration of the proteins in the cell based on
280 IFA, as well as with a lower sensitivity of ExM due to dilution of epitopes stemming from specimen
281 expansion. Taken altogether, ExM reveals that TbPH1 and TbKifX2 bind to the MtQ element of the *T.*
282 *brucei* cytoskeleton.

283

284 **Depletion of TbPH1 and TbKifX2 causes prominent morphological defects to the posterior end of *T.***
285 ***brucei***

286 To assay the function of the novel kinesin TbKifX2 and its associated kinesin-like protein TbPH1, we
287 depleted their expression by doxycycline-induced RNAi in the cell line expressing TbPH1-V5 and
288 TbKifX2-HA. The downregulation of either protein alone only marginally affected the growth of *T.*
289 *brucei* in comparison to the non-induced cells, despite efficient depletion of each of the respective
290 tagged proteins (Fig. 6A, S4A Fig.). After 6 days of RNAi-silencing of TbKifX2, we fractionated the
291 cytoskeleton from the cytosol under low salt conditions (Fig. 6B). Consistent with 'MT sieving'
292 fractionation (Figs. 2A and 3C) and IFA (Figs 5A and 5B), western blot detection revealed TbKifX2-HA

293 and TbPH1-V5 in both cytoskeletal and cytosolic fractions in cells grown in the absence of
294 tetracycline, in which neither protein was downregulated (Fig. 6B). However, TbPH1 was
295 preferentially depleted from the cytoskeleton fraction upon TbKifX2 silencing. This result indicates
296 that TbKifX2 recruits TbPH1-V5 to the MtQ (Fig. 6B).

297 Since depletion of either TbKifX2 or TbPH1 alone did not yield any other discernible phenotype, we
298 decided to deplete both proteins simultaneously. The cell line, in which both proteins were
299 downregulated, showed more pronounced growth inhibition than the single knock-downs (Fig. 6A).
300 Growth slowed after 3 days of RNAi induction and did not reach levels of the uninduced
301 counterparts at any point during the 7 day time course (S4B Fig.). Depletion of both proteins was
302 confirmed by western blotting (S4C Fig.), although neither protein was decreased below the
303 detection limits of this assay.

304 Because both TbPH1 and TbKifX2 are modified in a way suggestive of post-translational regulation
305 (Fig. 1), plus both associate with proteins that may regulate the cell cycle (*e.g.* FP45) [13] and do play
306 a role in cytokinesis (*e.g.* TOEFAZ1/Cif1) [49,50]**,** we wondered whether the growth inhibition of the
307 double RNAi knockdown is due to a cell cycle defect. Thus, we assayed the proportion of cell cycle
308 stages present over a course of 7 days of TbPH1/TbKifX2 depletion, sorting individual DAPI-stained
309 cells into different cell cycle stages by scoring their number of nuclei (N) and kinetoplasts (K) [3]. The
310 proportion of 1N1K cells decreased while 2N2K cells doubled at the same time from around 10% of
311 the population to about 20% (S4D Fig.). The number of zoids (cells with 1 kinetoplast and lacking a
312 nucleus) reached a peak at day 5, making up about 7% of the population, which may suggest
313 problems with cytokinesis. However, we did not observe the consequent emergence of 2N1K or
314 multinucleated cells, arguing against a specific cytokinesis defect [3]. Thus, we conclude that TbKifX2
315 and TbPH1 likely do not play a direct role in cell cycle progression and cytokinesis, and thus looked
316 for other phenotypes that would explain the decreased fitness of these cells.

317 We assayed the MtQ and FAZ after 5 days of RNAi depletion and observed no defects in either of
318 these structures, indicating that TbPH1 and TbKifX2 do not play a role in their biogenesis (Fig. 6C).
319 The lack of an effect on these structures is also consistent with the notion that these proteins do not
320 have a role in cytokinesis. However, by phase contrast microscopy we noticed the emergence of two
321 morphological phenotypes, namely multiple cells joined together on their posterior end, a
322 phenotype resembling abscission defects [51,52] and single cells with protrusions from the posterior
323 end (Fig. 6D).

324 To better visualize these phenotypes, we observed these cells by scanning electron microscopy (Fig.
325 7). While control cells showed normal trypomastigote morphology and cytokinesis (Fig. 7), we
326 observed concatenated cells as well as cells with multiple protrusions (arrows) originating from the
327 posterior end (Fig. 7). It should be noted that this stunning phenotype, while frequently observed,
328 did not emerge in all RNAi-induced cells. The occurrence of these cell types was also corroboratively
329 found in transmission electron microscopy, which in addition provided evidence that these
330 protrusions appear to contain normal cellular contents and were surrounded by subpellicular MTs
331 (S5A Fig.). Moreover, the flagellar pocket region appeared to be unaffected by depletion of
332 TbPH1/TbKifX2 (S5B and C Fig.).

333 This effect of TbPH1/TbKifX2-depletion resembled that of two tubulin-tyrosine-ligase-like (TTLL)
334 proteins, which post-translationally modify the C-terminal tails of α- and β-tubulin by addition of
335 polyglutamate side chains [53]. Upon depletion of either TTLL, protrusions were observed emanating
336 from the posterior end, which prompted the authors to name this morphological change the 'glove'
337 phenotype. To determine whether TbPH1/TbKifX2 downregulation truly phenocopies that of each
338 TTLL, we immunodecorated cells 5 days post RNAi-induction with antibodies recognizing glutamyl
339 side chains (GT335 antibody) and tyrosinated α-tubulin (YL 1/2 antibody); the latter antibody was
340 used previously to visualize the basal bodies (Fig. 5C). Upon depletion of either TTLL,
341 polyglutamylation was decreased and α-tubulin tyrosination increased in the posterior end, from

342 which the protrusions emerged [53]. We did not observe either of these changes in post-
343 translational modifications upon TbPH1/TbKifX2 silencing by observing them on individual cells by
344 IFA (S5D Fig.) or the whole cell population by western analysis (S5E Fig.), suggesting the mechanism
345 underlying the emergence of posterior-end protrusions differs from that of the TTLLs.

346

347 **DISCUSSION**

348 Kinesins and related kinesin-like proteins constitute one of the largest protein families encoded by
349 the *T. brucei* genome [16] and are represented by diverse gene repertoires in other trypanosomatids
350 as well [17–20]. Among the eukaryotes, trypanosomatids have experienced one of the largest
351 expansions of the kinesin motor superfamily, suggesting these proteins endow trypanosomes with
352 unique biological properties, many of which still await elucidation [16,19,20]. Indeed, this expansion
353 has resulted in the emergence of two trypanosomatid-specific clades of kinesins, named X-1 and X-2.
354 A kinesin belonging to the former, named FCP2/TbKinX1, has been shown to maintain a connection
355 of a new flagellum's distal tip along the side of the old flagellum, thus facilitating the unique
356 mechanism of templated replication of this cytoskeletal organelle in *T. brucei* [29].

357 In this work, we have shed light on the function of a member of the trypanosomatid-specific X-2
358 clade, which we named TbKifX2. We show that TbKifX2 is localized to the MtQ component of the
359 cytoskeleton while maintaining a cytosolic fraction. Previously, TbSpef1 [13] and three other
360 proteins of the TbSpef1 proxisome [14] were found to be localized to the MtQ of kinetoplastids.
361 However, these proteins are located exclusively on the proximal end of the MtQ, in the region
362 between the basal body and the flagellar collar. While TbKifX2 is enriched in this part of the MtQ,
363 this is to our knowledge the first protein identified to be also distributed along the entire length of
364 the MtQ.

365 TbKifX2 recruits TbPH1, a kinesin-like protein with a C-terminal PH domain, to the MtQ. The
366 proposed complex formation is based on our observation that TbPH1 mainly interacts with TbKifX2
367 with a strong affinity that defies high salt concentrations, a condition that usually subverts non-
368 covalent interactions between the CC domains [54]. It is not unusual for a kinesin to interact with
369 proteins that have a catalytically-dead kinesin motor domain [55] and we hypothesize that this
370 complex may represent an adaptation for binding the MtQ. How the TbKifX2/TbPH1 complex
371 preferentially interacts with the MtQ over the corset microtubules is an intriguing question. It has
372 been suggested that the MtQ contains β-tubulin with a unique but still unknown modification that is
373 recognized by the 1B41 monoclonal antibody [44,56], and could have an increased affinity to the
374 kinesin complex investigated here. Alternatively, the kinesins could be activated at a specific site, for
375 example at the proximal end of the MtQ, similar to the yeast kinesin Kip2 being recruited to the
376 minus ends of microtubules by the activity of the spindle pole bodies [57]. Whether this is indeed
377 the case, and how such a complex would move along the MtQ [55], remain interesting questions for
378 future research.

379 The TbPH1 proxisome obtained *via* BioID labelling revealed interesting properties of TbPH1 and
380 TbKifX2. First, most of the proteins identified in our study were also observed in the TOEFAZ1/CIF1
381 proxisome with high confidence [28]. This verifies our localization of TbKifX2/TbPH1 along the whole
382 length of the MtQ and not just the proximal end, since TOEFAZ1/CIF1 is enriched in the distal tip of a
383 newly formed FAZ, which also incorporates a new MtQ [8,58]. Second, the TbPH1 proxisome
384 contains DLP1/2, which are involved in clathrin-mediated endocytosis [41–43] and FP45, which
385 surrounds the flagellar pocket where endocytosis takes place. This result suggests that TbPH1 may
386 transport vesicular cargo, as PH domains have been shown to bind phosphoinositides, ubiquitous
387 phospholipids that pepper cellular membranes [59]. Interestingly, another kinesin with a C-terminal
388 PH domain was also found in the TbPH1 proxisome. Third and finally, a putative flavin-trafficking
389 protein was also found to associate with TbPH1 and TOEFAZ1/CIF1 [28]. This annotation is based on
390 the presence of an ApbE-like domain, which is common in prokaryotes but a rare occurrence in

391 eukaryotic proteins [60]. What an enzyme potentially influencing redox is doing in association with
392 the MtQ is another open question that has been uncovered in this study.

393 Simultaneous depletion of TbPH1 and TbKifX2 does not affect the overall morphology of MtQ or FAZ,
394 indicating these proteins are likely not involved in the biogenesis of these cellular structures. As
395 these single copy organelles must be faithfully replicated during cell proliferation, it is not surprising
396 that the impact of the double knockdown had a minimal impact on the cell cycle. Nevertheless,
397 TbKifX2/ TbPH1 downregulation has a striking morphogenesis phenotype, namely the accumulation
398 of protrusions from the posterior end of *T. brucei*. The intracellular contents of these protrusions
399 appear to be comparable to the rest of the cell and they are also surrounded by subpellicular MTs.
400 Interestingly, these protrusions are reminiscent of the 'glove phenotype' observed upon depletion of
401 two TTLL enzymes, which are responsible for post-translational modifications appending the C-
402 terminal tails of α- and β-tubulin [53].

403 However, at this juncture, we can only speculate about the nature of these posterior protrusions.
404 For one, simultaneous TbPH1 and TbKifX2 depletion did not affect polyglutamylation or tyrosination
405 of tubulins, indicating that these proteins do not play a role in regulating either of these post-
406 translational modifications as is the case for either TTLL [53]. Malfunction of regulated
407 polyglutamylation and tyrosination led to mislocalization of EB1, a MT-plus-end-binding protein that
408 binds to the MT corset at the posterior tip [53,61]. It was proposed that EB1 proteins may dock onto
409 tubulins with the aforementioned post-translational modifications [53]. So, the malformations seen
410 in TbPH1/TbKifX2 may affect EB1 or other such MT-plus-end-binding proteins, leading to
411 uncontrolled MT growth or aberrant MT organization. However, it should be noted that EB1 was not
412 identified in the TbPH1 proxisome, so any effect on this protein may be an indirect consequence of
413 RNAi-silencing. The protrusions may also be a consequence of delayed or uncoordinated cytokinesis
414 or represent mechanical damage to the posterior ends due to faulty separation of daughter cells at
415 the final stage of cytokinesis. However, arguing against protrusions arising from a putative

416 cytokinesis defect is that they were not observed in *T. brucei* unable to pull apart due to motility
417 defects [52].

418 In summary, we propose the following model (Fig. 8): the TbPH1-TbKifX2 complex moves along the
419 MtQ transporting cargo representing an auxiliary factor for inducing and/or executing cytokinesis at
420 the distal end of FAZ/MtQ. We assume that TbKifX2 is a plus-end directed motor based on the N-
421 terminal position of the kinesin motor domain in the molecule [36]. When TbPH1-TbKifX2 are
422 depleted, this cargo does not reach the anterior end and potentially accumulates at the posterior of
423 the cell instead, thereby causing aberrant organizations of MTs, resulting in the observed
424 protrusions. In the remote possibility that TbKifX2 moves toward the minus end of the MtQ MTs, we
425 propose that this hypothetical factor may regulate proper posterior end remodelling post
426 cytokinesis. In this case, TbPH1-TbKifX2 depletion impedes delivery of this cargo to the posterior
427 end, resulting in aberrant remodelling as exemplified by the observed protrusions. In conclusion, we
428 have discovered a novel kinesin heterocomplex that localizes along the MtQ, which will facilitate
429 understanding of this fascinating structure and how it may impact the gross morphology of
430 trypanosomatids.

431

432 **MATERIALS AND METHODS**

433 **Cells**

434 Procyclic SmOxP9 cells [62] were grown in SDM79 with 1 µg/ml of puromycin. Cell lines bearing
435 epitope tags were grown with 50 µg /ml hygromycin (TbPH1-V5), 15 µg /ml G418 (TbKifX2-HA) and
436 10 µg /ml blasticidin (TbPH1-BioID2-HA). Selection for RNAi constructs was with 2.5 µg /ml
437 phleomycin (TbKifX2 RNAi, TbPH1 RNAi and TbKifX2+TbPH1 RNAi).

438 **Plasmids and generation of cell lines**

439 For epitope tagging at the endogenous locus with HA and V5, long PCR products were generated
440 with primers TbPH1V5 FW (TTTCTTCCGGTCTTGACTTATTCCGCTCAGGGAAGCTTTATGATTTCTTATGCGA
441 AAAGAGAGTCATACCGCTCCCGTACggttctggtagtggttcc) and TbPH1V5 RV (ATAATAAAGAGGAAGGGAAG
442 GTAAAGTTCAGAAACAAATTCTGTTGGCTCCTGATAACACTCTCATATTTCCTTCACCGCccaatttgagagacctgtg
443 c) and primers TbKifX2HA FW (TTTCTTCCGGTCTTGACTTATTCCGCTCAGGGAAGCTTTATGATTTCTTATGC
444 GAAAAGAGAG TCATACCGCTCCCGTACggttctggtagtggttcc) and TbKifX2HA RV (ATAATAAAGAGGAAGG
445 GAAGGTAAAGTTCAGAAACAAATTCTGTTGGCTCCTGATAACACTCTCATATTTCCTTCACCGCccaatttgagaga
446 cctgtgc) using pPOT-V5-HygR and pPOT-HA-NeoR vectors as templates (based on [63] and modified
447 from pPOTv4 [33]). For tagging with the BioID2 ligase [38], a modified version of pPOTv7-Blast-mNG
448 [39] was used with the aforementioned primers for TbPH1 endogenous locus tagging. 50 µl PCR
449 reactions were directly transfected into procyclic SmOxP9 cells using the Amaxa Nucleofactor
450 electroporator and selection occurred approximately 16 hours after electroporation.

451 To create a vector to simultaneously downregulate both TbPH1 and TbKifX2, a fragment of each (as
452 suggested by RNAit2 software (https://dag.compbio.dundee.ac.uk/RNAit/) [64]) was PCR amplified
453 using primers TbPH1-RNAi-Fw (TAATtctagaGTTGCGTGATGAGCTTCAAA), TbPH1-RNAi-Rv
454 (TATAaagcttCTCCTCTAGCACCGTTTTGC), TbKifX2-RNAi-Fw (TAATggatccCACCGCCATTCTGCA AACAA)
455 and TbKifX2-RNAi-Rv (TATAtctagaGTCATTTGCGTGGGCGATAC) and cloned into BamHI-HindIII sites of
456 p2T7-177 [65] in a three way ligation using XbaI as the restriction site in between the two RNAi
457 fragments. The plasmid was linearised with NotI before electroporation.

458 **RNAi and growth curves**

459 Procyclic form cell lines for depletion of either TbPH1 or TbKifX2 were induced at a density of $2x10^6$
460 cells/ml with 1 µg/ml doxycycline and growth monitored daily with a Z2 Coulter Counter Analyzer
461 (Beckman Coulter). Cells were diluted back to the initial cell density every day. Cell lines carrying the
462 vector for simultaneous depletion of TbPH1 and TbKifX2 were induced at a density of $5x10^5$ cells/ml

463 with 1 µg/ml doxycycline and growth monitored daily with a Neubauer counting chamber. Cells were
464 diluted back to the initial cell density every two days.

465 **DAPI counts**

466 For cell cycle analysis, cells either induced or not for depletion of TbKifX2 and TbPH1 were spread on
467 glass slides, the cell suspension allowed to air-dry and the slides then fixed in methanol at -20 °C.
468 Slides were rehydrated for 5 minutes in PBS before a drop of ProLong™ Gold antifade reagent with
469 DAPI (ThermoScientific) was added, a coverslip applied and the slide sealed. At least 200 cells were
470 scored according to the number of nuclei and kinetoplasts per slide.

471 **Cell fractionation via 'microtubule sieving'**

472 To entrap non-soluble and cytoskeletal proteins within the MT corset, a 'MT sieving' technique as
473 described in [32] was employed. The experiment was conducted exactly as described before in [32]
474 (see also S1 Fig.).

475 **V5 immunoprecipitation**

476 For immunoprecipitation (IP) of TbPH1-V5 from procyclic trypanosome lysates, the V5 antibody
477 (Thermo Fisher) was coupled and cross-linked to protein G coated dynabeads (Thermo Scientific)
478 using 6 mg/ml dimethyl pimelidate dihydrochloride in 0.2M triethanolamine. Beads were then
479 washed in IP wash buffer (20 mM Tris-HCl, pH 7.7, 100 mM KCl, 3 mM $MgCl_2$, 0.5% TritonX-100,
480 cOmplete™ EDTA-free protease inhibitor (Roche)) and stored at 4 °C before further usage. For
481 proteomic analysis of TbPH1 interactions, $1x10^9$ PCF cells were pre-fractionated using the 'MT
482 sieving' technique described above. The SN3 lysate was incubated with V5-coupled dynabeads for 24
483 hours at 4 °C. Following several washes in IP wash buffer, proteins were eluted using low pH glycine
484 buffer. Aliquots were taken of the different steps for western blot analysis.

485 **Western blots**

486 Cell lysates were prepared by boiling in 1x SDS sample buffer and the equivalent of $2x10^6$ cells (RNAi
487 lines) or $1x10^7$ cells (IP samples) was loaded per well. Following western blotting, PVDF membranes
488 were blocked for 1 hour in 5% milk-PBS. Incubation with primary antibodies (anti-V5 at 1:1,000;
489 ThermoScientific, anti-HA at 1:1,000; ThermoScientific, anti-tubulin at 1:5,000; Sigma) was
490 performed at 4 °C overnight. Secondary antibodies (HRP-coupled anti-mouse or –rabbit IgG; Sigma)
491 were used at a concentration of 1:2,000 and signals were visualised using Clarity Western ECL
492 substrate (Bio-Rad) on a ChemiDoc MP (Bio-Rad).

493 **SYPRO Ruby staining**

494 Following electrophoresis, polyacrylamide gels were placed into fixing solution (7% glacial acetic
495 acid, 50% methanol) for 30 minutes at room temperature. Following another, identical fixation step,
496 the gel was incubated with SYPRO Ruby solution overnight at room temperature. A washing step in
497 washing solution (7% glacial acetic acid, 10% methanol) for 30 minutes at room temperature was
498 followed by three 5 minute washes in milliQ water before imaging on a ChemiDoc MP (Bio-Rad).

499 **Immunofluorescence and cytoskeleton extraction**

500 Approximately $2x10^6$ cells were used per slide. Cells were washed in PBS and fixed in 2.3% PFA in PBS
501 for approximately 30 minutes before being transferred to microscopy slides (ThermoScientific).
502 Following neutralisation in 0.1M glycine in PBS, slides were incubated in methanol at -20° C
503 overnight for permeabilisation. Slides were then rehydrated in PBS and blocked in 1% BSA in PBS for
504 1 hour followed by incubation with primary antibody for 1 hour in a humid chamber. The slides were
505 then washed three times with PBS before incubation in AlexaFluor-conjugated secondary antibody
506 (goat anti-rabbit/mouse, used at 1:1,000; Invitrogen). Following three further washes in PBS, a drop
507 of ProLong Gold Antifade reagent with DAPI (ThermoScientific) was added, a coverslip applied and
508 the slide sealed with nail polish. Slides were imaged with a Zeiss Axioscope or an Olympus FluoView
509 Fv1000 confocal microscope.

510 For immunofluorescence analysis of cells extracted using the 'MT sieving' fractionation method
511 described above the pellet fraction P2 was fixed in 2.3% PFA as described. All subsequent steps were
512 the same as for whole cell immunofluorescence.

513 To extract cytoskeletons conventionally, approximately 1x 10^7 PCF cells were collected and
514 centrifuged at room temperature for 5 min at 800 x g and the supernatant discarded. Thereafter, the
515 cell pellet was washed once in PBS and after resuspension in PBS applied in a drop-wise fashion to
516 Superfrost plus® slides (ThermoScientific). The cells were left to settle before the addition of PEME
517 buffer (100 mM Pipes, pH 6.9, 1 mM $MgSO_4$, 2 mM EGTA, 0.1 mM EDTA) containing 0.5% (v/v) NP-40
518 (Igepal) for 10 seconds. This cytoskeleton extraction was followed by a 10 minute fixation step in 4%
519 PFA/-20°C methanol. All subsequent steps were as described above for whole cell
520 immunofluorescence.

521 Antibodies used in immunofluorescence

Antibody	Dilution	Origin
anti-HA (produced in rabbit)	1:1,000	Sigma, Catalog #: H6908
anti-V5 (produced in mouse)	1:1,000	ThermoScientific, Catalog #: 377500
1B41 (MtQ)[1]	1:1,000	[44]
L3B2	1:10	[66]
YL1/2	1:50	[67]
GT335	1:2,000	Adipogen Life Sciences, Catalog #: AG-20B-0020
[1]IgM purified from hybridoma supernatant and not mouse ascitic fluid as in original report.		

522

523 **Scanning and transmission electron microscopy**

524 For TEM, cell pellets were high-pressure frozen, freeze substituted in the presence of 2% OsO4 in
525 acetone, and embedded into Spi-Pon812 resin (SPI) as described previously [63]. For SEM of the
526 TbPH1/TbKifX2 RNAi cell line, cells were fixed in 2.5% glutaraldehyde in 100 mM PBS overnight at
527 4°C and then spotted onto poly-l-lysine-coated glass cover slips. The cells were post-fixed in 2%
528 osmium tetroxide in 100 mM PBS for 1 h at room temperature and finally washed in the same
529 buffer. After dehydration cells were critical-point dried, coated with gold palladium and imaged.

530 **Expansion microscopy**

531 Expansion microscopy samples were prepared as described previously [47]. In brief, $1x10^6$ cells were
532 fixed overnight in a solution containing 4% formaldehyde and 4% acrylamide in PBS and adhered to a
533 poly-L-lysine (Sigma, P4707) coated coverslip. The cells were gelated for 30 min at 37°C in PBS
534 supplemented with 19% sodium acrylate, 10% acrylamide, and 0.1% N, N'-Methylenebisacrylamide,
535 0.5% N, N, N´, N´-tetramethylethylenediamine, and 0.5% ammonium persulfate. The specimens
536 were further denatured by a 2 hour incubation at 95°C in a buffer consisting of 50 mM
537 tris(hydroxymethyl)aminomethane-hydrochloride, 200 mM sodium chloride, 200 mM sodium
538 dodecyl sulphate, pH 9.0, and expanded by three 20 min incubations with 15 ml of ultrapure water.

539 Thereafter, the gels were incubated overnight first with a mixture of anti-HA (Cell Signaling
540 Technology, 3724S; used at 1:250) and C3B9 (68, used at 1:10), anti-V5 (Sigma, V8137-.2MG; used at
541 1:250) and C3B9 or anti-ClpGM6 (48, used at 1:200) and C3B9 antibodies, followed by washes and an
542 overnight incubation with a mixture of secondary antibodies (Invitrogen, A11001 and A21428; used
543 at 1:500). Both primary and secondary antibodies were diluted in PBS supplemented with 2% bovine
544 serum albumin. Finally, the gels were washed with ultrapure water.

545 Prior to imaging, pieces of gels containing stained expanded cells was transferred to a glass-bottom
546 dish coated with poly-L-lysine, and imaged using a Leica TCS SP8 confocal microscope with an HC PL
547 apochromatic 63x/NA 1.40 oil immersion objective. Z-stacks were acquired with the step size of 100

548 nm. Confocal z-stacks were processed in Fiji [69]. 3D reconstructions were performed in the 3D
549 viewer plugin.

550 **BioID**

551 PCF cells (TbPH1-BioID2-HA and SmOxP9 as controls) were grown in the presence of 50 µM biotin for
552 24 hours. For proximity-dependent biotin identification (BioID), 10^9 PCF cells were extracted in PEME
553 buffer (100 mM Pipes, pH 6.9, 1 mM $MgSO_4$, 2 mM EGTA, 0.1 mM EDTA) containing 0.5% (v/v) NP-40
554 (Igepal) for 15 minutes at room temperature resulting in extract E1. Following centrifugation at
555 3,400 x g for 2 minutes, supernatant S1 was created and pellet P1 was further processed by
556 extraction in lysis buffer (0.4% SDS, 500 mM NaCl, 5 mM EDTA, 1 mM DTT, 50 mM Tris-HCl, pH7.4).
557 Another centrifugation step at 16,000 x g for 10 minutes created supernatant S2. Both supernatants,
558 S1 and S2, were then incubated with streptavidin-conjugated Dynabeads (company) for 4 hours at 4
559 °C. An aliquot of flow through samples F1 and F2 were retained for western blotting and the
560 dynabeads were washed five times with PBS. A small sample of the beads was then resuspended in
561 2x SDS PAGE buffer and boiled for initial western blot analysis. For mass spectrometry analysis of the
562 TbPH1 proxisome, the procedure was repeated as described above, but only the S1 fraction was
563 further processed.

564 **Mass spectroscopy analysis of captured biotinylated proteins**

565 Trypsin-digestion of captured biotinylated proteins was performed on bead prior to liquid
566 chromatography-tandem mass spectroscopy (LC-MS/MS) as previously described [39]. Data was
567 processed using MaxQuant [70] version 1.6.14 which incorporates the Andromeda search engine
568 [71]. Proteins were identified by searching a protein sequence database containing *T. brucei brucei*
569 927 annotated proteins (Version 51, TriTrypDB [25], http://www.tritrypdb.org/) supplemented with
570 frequently observed contaminants. Search parameters specified an MS tolerance of 6 ppm, an
571 MS/MS tolerance at 0.5 Da and full trypsin specificity, allowing for up to two missed cleavages.
572 Carbamidomethylation of cysteine was set as a fixed modification and oxidation of methionine and

573 N-terminal protein acetylation were allowed as variable modifications. The experimental design
574 included matching between runs for biological replicates. Peptides were required to be at least 7
575 amino acids in length, with false discovery rates (FDRs) of 0.01 calculated at the levels of peptides,
576 proteins and modification sites based on the number of hits against the reversed sequence
577 database. The obtained data was subsequently processed in Perseus version 1.6.14 as described in
578 [72].

579 **Data availability**

580 The mass spectrometry proteomics data have been deposited to the ProteomeXchange Consortium
581 via the PRIDE partner repository with the dataset identifier PXD025802.

582 **ACKNOWLEDGEMENTS**

583 We thank Keith Gull (University of Oxford), Linda Kohl (Muséum National d'Histoire Naturelle), Bill
584 Wickstead (University of Nottingham), and Ziyin Li (University of Texas Medical School at Houston)
585 for helpful comments, Susanne Kramer (University of Würzburg), Cynthia He (National University of
586 Singapore), and Chris de Graffenried (Brown University) for antibodies, Peter Gorilak (Institute of
587 Molecular Genetics) for assistance with imaging, as well as Karel Harant and Pavel Talacko (BIOCEV,
588 Prague) and Zbyněk Zdráhal and David Potěšil (CEITEC, Brno) for mass spectroscopy analysis on BioID
589 samples and excised bands, respectively. This work was supported by the Czech Science Foundation
590 grants 20-23513S to HH, and 21-09283S and ERC CZ LL1601 to JL, the ERD funds of the Czech
591 Ministry of Education 16_019/0000759 to HH and JL, and BioImaging grant LM2018129 to MV. Work
592 in the VV laboratory was supported by an EMBO Installation Grant and by the J. E. Purkyne
593 Fellowship of the Czech Academy of Sciences. The funders had no role in study design, data
594 collection and analysis, decision to publish, or preparation of the manuscript.

595

596 **REFERENCES**

597 1. Wheeler RJ, Scheumann N, Wickstead B, Gull K, Vaughan S. Cytokinesis in *Trypanosoma*
598 *brucei* differs between bloodstream and tsetse trypomastigote forms: implications for
599 microtubule-based morphogenesis and mutant analysis. Mol Microbiol. 2013;90: 1339–1355.
600 doi:10.1111/mmi.12436

601 2. Gull K. The cytoskeleton of trypanosomatid parasites. Annual Review of Microbiology. Annu
602 Rev Microbiol; 1999. pp. 629–655. doi:10.1146/annurev.micro.53.1.629

603 3. Robinson DR, Sherwin T, Ploubidou A, Byard EH, Gull K. Microtubule polarity and dynamics in
604 the control of organelle positioning, segregation, and cytokinesis in the trypanosome cell
605 cycle. J Cell Biol. 1995;128: 1163–1172. doi:10.1083/jcb.128.6.1163

606 4. Sherwin T, Gull K. Visualization of detyrosination along single microtubules reveals novel
607 mechanisms of assembly during cytoskeletal duplication in trypanosomes. Cell. 1989;57: 211–
608 221. doi:10.1016/0092-8674(89)90959-8

609 5. Field MC, Carrington M. The trypanosome flagellar pocket. Nat Rev Micro. 2009;7: 775–786.
610 Available: http://dx.doi.org/10.1038/nrmicro2221

611 6. Albisetti A, Florimond C, Landrein N, Vidilaseris K, Eggenspieler M, Lesigang J, et al.
612 Interaction between the flagellar pocket collar and the hook complex via a novel
613 microtubule-binding protein in *Trypanosoma brucei*. PLoS Pathog. 2017;13: e1006710.
614 doi:10.1371/journal.ppat.1006710

615 7. Lacomble S, Vaughan S, Gadelha C, Morphew MK, Shaw MK, McIntosh JR, et al. Three-
616 dimensional cellular architecture of the flagellar pocket and associated cytoskeleton in
617 trypanosomes revealed by electron microscope tomography. J Cell Sci. 2009;122: 1081–1090.
618 doi:10.1242/jcs.045740

619 8. Sunter JD, Gull K. The Flagellum Attachment Zone: 'The Cellular Ruler' of Trypanosome
620 Morphology. Trends in Parasitology. Elsevier Ltd; 2016. pp. 309–324.

621 doi:10.1016/j.pt.2015.12.010

622 9. Sinclair AN, de Graffenried CL. More than Microtubules: The Structure and Function of the
623 Subpellicular Array in Trypanosomatids. Trends in Parasitology. Elsevier Ltd; 2019. pp. 760–
624 777. doi:10.1016/j.pt.2019.07.008

625 10. Wheeler RJ, Gull K, Sunter JD. Coordination of the cell cycle in trypanosomes. Annu Rev
626 Microbiol. 2019;73: 133–154. doi:10.1146/annurev-micro-020518-115617

627 11. Woodward R, Gull K. Timing of nuclear and kinetoplast DNA replication and early
628 morphological events in the cell cycle of *Trypanosoma brucei*. J Cell Sci. 1990;95 (Pt 1): 49–
629 57. Available: http://www.ncbi.nlm.nih.gov/pubmed/2190996

630 12. Lacomble S, Vaughan S, Gadelha C, Morphew MK, Shaw MK, McIntosh JR, et al. Basal body
631 movements orchestrate membrane organelle division and cell morphogenesis in
632 *Trypanosoma brucei*. J Cell Sci. 2010;123: 2884–2891. doi:10.1242/jcs.074161

633 13. Gheiratmand L, Brasseur A, Zhou Q, He CY. Biochemical characterization of the bi-lobe reveals
634 a continuous structural network linking the bi-lobe to other single-copied organelles in
635 *Trypanosoma brucei*. J Biol Chem. 2013;288: 3489–3499. doi:10.1074/jbc.M112.417428

636 14. Dong X, Lim TK, Lin Q, He CY. Basal Body Protein TbSAF1 Is Required for Microtubule Quartet
637 Anchorage to the Basal Bodies in *Trypanosoma brucei*. Hajduk SL, editor. mBio. 2020;11:
638 e00668-20. doi:10.1128/mBio.00668-20

639 15. Hirokawa N, Noda Y. Intracellular transport and kinesin superfamily proteins, KIFs: Structure,
640 function, and dynamics. Physiol Rev. 2008;88: 1089–1118. doi:10.1152/physrev.00023.2007

641 16. Berriman M, Ghedin E, Hertz-Fowler C, Blandin G, Renauld H, Bartholomeu DC, et al. The
642 genome of the African trypanosome *Trypanosoma brucei*. Science. 2005;309: 416–422.
643 doi:10.1126/science.1112642

644 17. El-Sayed NM, Myler PJ, Bartholomeu DC, Nilsson D, Aggarwal G, Tran AN, et al. The genome
645 sequence of *Trypanosoma cruzi*, etiologic agent of Chagas disease. Science. 2005;309: 409–
646 415. doi:10.1126/science.1112631

647 18. Ivens AC, Peacock CS, Worthey EA, Murphy L, Aggarwal G, Berriman M, et al. The genome of
648 the kinetoplastid parasite, *Leishmania major*. Science. 2005;309: 436–442.
649 doi:10.1126/science.1112680

650 19. Wickstead B, Gull K, Richards TA. Patterns of kinesin evolution reveal a complex ancestral
651 eukaryote with a multifunctional cytoskeleton. BMC Evol Biol. 2010;10:
652 https://doi.org/10.1186/1471-2148-10-110. doi:10.1186/1471-2148-10-110

653 20. Wickstead B, Gull K. A "Holistic" Kinesin Phylogeny Reveals New Kinesin Families and Predicts
654 Protein Functions. Mol Biol Cell. 2006;17: 1734–1743. doi:10.1091/mbc.E05

655 21. Li Z, Lee JH, Chu F, Burlingame AL, Günzl A, Wang CC. Identification of a Novel Chromosomal
656 Passenger Complex and Its Unique Localization during Cytokinesis in *Trypanosoma brucei*.
657 Carlow CKS, editor. PLoS One. 2008;3: e2354. doi:10.1371/journal.pone.0002354

658 22. Wickstead B, Carrington JT, Gluenz E, Gull K. The expanded kinesin-13 repertoire of
659 trypanosomes contains only one mitotic kinesin indicating multiple extra-nuclear roles. PLoS
660 One. 2010;5: e0015020. doi:10.1371/journal.pone.0015020

661 23. Hu L, Hu H, Li Z. A kinetoplastid-specific kinesin is required for cytokinesis and for
662 maintenance of cell morphology in *Trypanosoma brucei*. Mol Microbiol. 2012;83: 565–578.
663 doi:10.1111/j.1365-2958.2011.07951.x

664 24. Wei Y, Hu H, Lun Z-R, Li Z. The Cooperative Roles of Two Kinetoplastid-Specific Kinesins in
665 Cytokinesis and in Maintaining Cell Morphology in Bloodstream Trypanosomes. PLoS One.
666 2013;8: e73869. doi:10.1371/journal.pone.0073869

667 25. Aslett M, Aurrecoechea C, Berriman M, Brestelli J, Brunk BP, Carrington M, et al. TriTrypDB: A

668 functional genomic resource for the Trypanosomatidae. Nucleic Acids Res. 2009;38: D457–
669 D462. doi:10.1093/nar/gkp851

670 26. Bertiaux E, Morga B, Blisnick T, Rotureau B, Bastin P. A Grow-and-Lock Model for the Control
671 of Flagellum Length in Trypanosomes. Curr Biol. 2018;28: 3802-3814.e3.
672 doi:10.1016/j.cub.2018.10.031

673 27. An T, Li Z. An orphan kinesin controls trypanosome morphology transitions by targeting
674 FLAM3 to the flagellum. Hill KL, editor. PLOS Pathog. 2018;14: e1007101.
675 doi:10.1371/journal.ppat.1007101

676 28. Hilton NA, Sladewski TE, Perry JA, Pataki Z, Sinclair-Davis AN, Muniz RS, et al. Identification of
677 TOEFAZ1-interacting proteins reveals key regulators of *Trypanosoma brucei* cytokinesis. Mol
678 Microbiol. 2018;109: 306–326. doi:10.1111/mmi.13986

679 29. Varga V, Moreira-Leite F, Portman N, Gull K. Protein diversity in discrete structures at the
680 distal tip of the trypanosome flagellum. Proc Natl Acad Sci U S A. 2017;114: E6546–E6555.
681 doi:10.1073/pnas.1703553114

682 30. Urbaniak MD, Guther MLS, Ferguson M a J. Comparative SILAC proteomic analysis of
683 *Trypanosoma brucei* bloodstream and procyclic lifecycle stages. PLoS One. 2012;7: e36619.
684 doi:10.1371/journal.pone.0036619

685 31. Lott K, Li J, Fisk JC, Wang H, Aletta JM, Qu J, et al. Global proteomic analysis in trypanosomes
686 reveals unique proteins and conserved cellular processes impacted by arginine methylation. J
687 Proteomics. 2013;91: 210–225. doi:10.1016/j.jprot.2013.07.010

688 32. Fritz M, Vanselow J, Sauer N, Lamer S, Goos C, Siegel TN, et al. Novel insights into RNP
689 granules by employing the trypanosome's microtubule skeleton as a molecular sieve. Nucleic
690 Acids Res. 2015;43: 8013–8032. doi:10.1093/nar/gkv731

691 33. Dean S, Sunter J, Wheeler RJ, Hodkinson I, Gluenz E, Gull K. A toolkit enabling efficient,

692 scalable and reproducible gene tagging in trypanosomatids. Open Biol. 2015;5: 140197.
693 doi:10.1098/rsob.140197

694 34. Marx A, Hoenger A, Mandelkow E. Structures of kinesin motor proteins. Cell Motil
695 Cytoskeleton. 2009;66: 958–966. doi:10.1002/cm.20392

696 35. Burkhard P, Stetefeld J, Strelkov S V. Coiled coils: A highly versatile protein folding motif.
697 Trends in Cell Biology. Trends Cell Biol; 2001. pp. 82–88. doi:10.1016/S0962-8924(00)01898-5

698 36. Hirokawa N, Noda Y, Tanaka Y, Niwa S. Kinesin superfamily motor proteins and intracellular
699 transport. Nature Reviews Molecular Cell Biology. Nature Publishing Group; 2009. pp. 682–
700 696. doi:10.1038/nrm2774

701 37. Dean S, Sunter JD, Wheeler RJ. TrypTag.org: A Trypanosome Genome-wide Protein
702 Localisation Resource. Trends in Parasitology. Elsevier Ltd; 2017. pp. 80–82.
703 doi:10.1016/j.pt.2016.10.009

704 38. Kim DI, Jensen SC, Noble KA, Kc B, Roux KH, Motamedchaboki K, et al. An improved smaller
705 biotin ligase for BioID proximity labeling. Mol Biol Cell. 2016;27: 1188–1196.
706 doi:10.1091/mbc.E15-12-0844

707 39. Pyrih J, Rašková V, Škodová-Sveráková I, Pánek T, Lukeš J. ZapE/Afg1 interacts with Oxa1 and
708 its depletion causes a multifaceted phenotype. PLoS One. 2020;15: e0234918.
709 doi:10.1371/journal.pone.0234918

710 40. Morriswood B, Havlicek K, Demmel L, Yavuz S, Sealey-Cardona M, Vidilaseris K, et al. Novel
711 bilobe components in *Trypanosoma brucei* identified using proximity-dependent
712 biotinylation. Eukaryot Cell. 2013;12: 356–367. doi:10.1128/EC.00326-12

713 41. Benz C, Stříbrná E, Hashimi H, Lukeš J. Dynamin-like proteins in *Trypanosoma brucei*: A
714 division of labour between two paralogs? PLoS One. 2017;12: e0177200.
715 doi:10.1371/journal.pone.0177200

716 42. Morgan GW, Goulding D, Field MC. The single dynamin-like protein of *Trypanosoma brucei*
717 regulates mitochondrial division and is not required for endocytosis. J Biol Chem. 2004;279:
718 10692–701. doi:10.1074/jbc.M312178200

719 43. Chanez A-L, Hehl AB, Engstler M, Schneider A. Ablation of the single dynamin of *T. brucei*
720 blocks mitochondrial fission and endocytosis and leads to a precise cytokinesis arrest. J Cell
721 Sci. 2006;119: 2968–74. doi:10.1242/jcs.03023

722 44. Gallo JM, Précigout E, Schrével J. Subcellular sequestration of an antigenically unique beta-
723 tubulin. Cell Motil Cytoskeleton. 1988;9: 175–183. doi:10.1002/cm.970090209

724 45. Gambarotto D, Zwettler FU, Le Guennec M, Schmidt-Cernohorska M, Fortun D, Borgers S, et
725 al. Imaging cellular ultrastructures using expansion microscopy (U-ExM). Nat Methods.
726 2019;16: 71–74. doi:10.1038/s41592-018-0238-1

727 46. Amodeo S, Kalichava A, Fradera-Sola A, Bertiaux-Lequoy E, Guichard P, Butter F, et al.
728 Characterization of the novel mitochondrial genome segregation factor TAP110 in
729 *Trypanosoma brucei*. J Cell Sci. 2021;134: jcs.254300. doi:10.1242/jcs.254300

730 47. Gorilak P, Pružincová M, Vachova H, Olšinová M, Varga V. Expansion microscopy facilitates
731 quantitative super-resolution studies of cytoskeletal structures in kinetoplastid parasites.
732 Open Biol. 2021;11: 210131. Available: https://doi.org/10.1101/2021.04.20.440601

733 48. Hayes P, Varga V, Olego-Fernandez S, Sunter J, Ginger ML, Gull K. Modulation of a
734 cytoskeletal calpain-like protein induces major transitions in trypanosome morphology. J Cell
735 Biol. 2014;206: 377–384. doi:10.1083/jcb.201312067

736 49. McAllaster MR, Ikeda KN, Lozano-Núñez A, Anrather D, Unterwurzacher V, Gossenreiter T, et
737 al. Proteomic identification of novel cytoskeletal proteins associated with TbPLK, an essential
738 regulator of cell morphogenesis in *Trypanosoma brucei*. Mol Biol Cell. 2015;26: 3013–3029.
739 doi:10.1091/mbc.E15-04-0219

740 50. Zhou Q, An T, Pham KTM, Hu H, Li Z. The CIF1 protein is a master orchestrator of
741 trypanosome cytokinesis that recruits several cytokinesis regulators to the cytokinesis
742 initiation site. J Biol Chem. 2018;293: 16177–16192. doi:10.1074/jbc.RA118.004888

743 51. Benz C, Clucas C, Mottram JC, Hammarton TC. Cytokinesis in bloodstream stage *Trypanosoma*
744 *brucei* requires a family of katanins and spastin. PLoS One. 2012;7: e30367.
745 doi:10.1371/journal.pone.0030367

746 52. Ralston KS, Lerner AG, Diener DR, Hill KL. Flagellar motility contributes to cytokinesis in
747 *Trypanosoma brucei* and is modulated by an evolutionarily conserved dynein regulatory
748 system. Eukaryot Cell. 2006;5: 696–711. doi:10.1128/EC.5.4.696-711.2006

749 53. Jentzsch J, Sabri A, Speckner K, Lallinger-Kube G, Weiss M, Ersfeld K. Microtubule
750 polyglutamylation is important for regulating cytoskeletal architecture and motility in
751 *Trypanosoma brucei*. J Cell Sci. 2020;133. doi:10.1242/jcs.248047

752 54. Grigoryan G, Keating AE. Structural specificity in coiled-coil interactions. Current Opinion in
753 Structural Biology. Curr Opin Struct Biol; 2008. pp. 477–483. doi:10.1016/j.sbi.2008.04.008

754 55. Allingham JS, Sproul LR, Rayment I, Gilbert SP. Vik1 Modulates Microtubule-Kar3 Interactions
755 through a Motor Domain that Lacks an Active Site. Cell. 2007;128: 1161–1172.
756 doi:10.1016/j.cell.2006.12.046

757 56. Gallo JM, Precigout E. Tubulin expression in trypanosomes. Biol Cell. 1988;64: 137–143.
758 doi:10.1016/0248-4900(88)90073-1

759 57. Chen X, Widmer LA, Stangier MM, Steinmetz MO, Stelling J, Barral Y. Remote control of
760 microtubule plus-end dynamics and function from the minus-end. Elife. 2019;8: 1–32.
761 doi:10.7554/eLife.48627

762 58. Campbell PC, de Graffenried CL. Alternate histories of cytokinesis: lessons from the
763 trypanosomatids. Mol Biol Cell. 2020;31: 2631–2639. doi:10.1091/mbc.E19-12-0696

764 59. Lemmon MA. Pleckstrin homology (PH) domains and phosphoinositides. Biochem Soc Symp.
765 2007;74: 81–93. doi:10.1042/BSS0740081

766 60. Schenk R, Bachmaier S, Bringaud F, Boshart M. Efficient flavinylation of glycosomal fumarate
767 reductase by its own ApbE domain in *Trypanosoma brucei*. FEBS J. 2021;
768 https://doi.org/10.1111/febs.15812. doi:10.1111/febs.15812

769 61. Sheriff O, Lim LF, He CY. Tracking the biogenesis and inheritance of subpellicular microtubule
770 in *Trypanosoma brucei* with inducible YFP- α-tubulin. Biomed Res Int. 2014;2014.
771 doi:10.1155/2014/893272

772 62. Poon SK, Peacock L, Gibson W, Gull K, Kelly S. A modular and optimized single marker system
773 for generating *Trypanosoma brucei* cell lines expressing T7 RNA polymerase and the
774 tetracycline repressor. Open Biol. 2012;2: 110037. doi:10.1098/rsob.110037

775 63. Kaurov I, Vancová M, Schimanski B, Cadena LR, Heller J, Bílý T, et al. The Diverged
776 Trypanosome MICOS Complex as a Hub for Mitochondrial Cristae Shaping and Protein
777 Import. Curr Biol. 2018;28: 3393-3407.e5. doi:10.1016/j.cub.2018.09.008

778 64. Redmond S, Vadivelu J, Field MC. RNAit: An automated web-based tool for the selection of
779 RNAi targets in *Trypanosoma brucei*. Mol Biochem Parasitol. 2003;128: 115–118.
780 doi:10.1016/S0166-6851(03)00045-8

781 65. Wickstead B, Ersfeld K, Gull K. Targeting of a tetracycline-inducible expression system to the
782 transcriptionally silent minichromosomes of *Trypanosoma brucei*. Mol Biochem Parasitol.
783 2002;125: 211–6. doi:10.1016/S0166-6851(02)00238-4

784 66. Kohl L, Sherwin T, Gull K. Assembly of the paraflagellar rod and the flagellum attachment
785 zone complex during the *Trypanosoma brucei* cell cycle. J Eukaryot Microbiol. 1999;46: 105–
786 109. doi:10.1111/j.1550-7408.1999.tb04592.x

787 67. Sherwin T, Schneider A, Sasse R, Seebeck T, Gull K. Distinct localization and cell cycle

788 dependence of COOH terminally tyrosinolated α-tubulin in the microtubules of *Trypanosoma*
789 *brucei brucei*. J Cell Biol. 1987;104: 439–446. doi:10.1083/jcb.104.3.439

790 68. Woods A, Sherwin T, Sasse R, MacRae TH, Baines AJ, Gull K. Definition of individual
791 components within the cytoskeleton of *Trypanosoma brucei* by a library of monoclonal
792 antibodies. J Cell Sci. 1989;93 (Pt 3): 491—500. Available:
793 http://europepmc.org/abstract/MED/2606940

794 69. Schindelin J, Arganda-Carreras I, Frise E, Kaynig V, Longair M, Pietzsch T, et al. Fiji: An open-
795 source platform for biological-image analysis. Nature Methods. Nature Publishing Group;
796 2012. pp. 676–682. doi:10.1038/nmeth.2019

797 70. Cox J, Mann M. MaxQuant enables high peptide identification rates, individualized p.p.b.-
798 range mass accuracies and proteome-wide protein quantification. Nat Biotechnol. 2008;26:
799 1367–1372. doi:10.1038/nbt.1511

800 71. Cox J, Neuhauser N, Michalski A, Scheltema RA, Olsen J V., Mann M. Andromeda: A peptide
801 search engine integrated into the MaxQuant environment. J Proteome Res. 2011;10: 1794–
802 1805. doi:10.1021/pr101065j

803 72. Zoltner M, del Pino RC, Field MC. Sorting the Muck from the Brass: Analysis of Protein
804 Complexes and Cell Lysates. Methods in Molecular Biology. Humana Press Inc.; 2020. pp.
805 645–653. doi:10.1007/978-1-0716-0294-2_38

806 73. Kramer S, Queiroz R, Ellis L, Webb H, Hoheisel JD, Clayton C, et al. Heat shock causes a
807 decrease in polysomes and the appearance of stress granules in trypanosomes independently
808 of eIF2α phosphorylation at Thr169. J Cell Sci. 2008;121: 3002–3014. doi:10.1242/jcs.031823

809 **Figure Legends**

810 **Fig. 1:** Domain architecture of TbPH1 and TbKifX2. Schematic depiction includes phosphorylation and
811 arginine methylation sites. The consensus Walker A motif is shown in comparison with the

812 respective motifs of TbPH1 and TbKifX2. Key residues in ATP hydrolysis shown in red and mutations
813 in purple. CC: coiled coil domain, PH: pleckstrin homology domain, HDL: homeodomain-like fold.

814 **Fig. 2:** TbPH1-V5 fractionates with the cytoskeleton. **(A)** Western blot of-trypanosome cell fractions.
815 Fractionation procedure is summarized in S1 Fig. Antibodies used were anti-V5 and anti-SCD6 [73]. T:
816 total lysate, SN: supernatant, P: pellet. **(B)** IFA of fraction P2. Cells were labelled with anti-V5
817 antibody (green) and DAPI. The scale bar corresponds to 5 µm.

818 **Fig. 3:** TbPH1 interacts with TbKifX2, a kinetoplastid-specific kinesin. **(A)** Western blot verifying
819 immunoprecipitation of TbPH1-V5. The blot was probed with anti-V5 and anti-α-tubulin antibodies.
820 The parental cell line SmOxP9 was used as a control. T: total lysate, SN3: supernatant 3, FT: flow
821 through, E: elution. **(B)** SyproRuby-stained gel of elution fractions of TbPH1-V5 IP and mock control
822 (SmOxP9). B1 and B2: bands excised and identified by mass spectrometry. **(C)** Western blot showing
823 interaction of TbPH1-V5 and TbKifX2-HA. TbKifX2-HA was immunoprecipitated in the same way as
824 PH1-V5. T: total lysate, SN: supernatant, P: pellet, FT: flow through, E: elution. **(D)** IFA on whole cells
825 detecting TbPH1-V5 (top) and TbKifX2-HA (bottom). Cells were counterstained with antibody
826 recognizing α-tubulin (top) and acetylated α-tubulin (bottom). The scale bar corresponds to 5 µm.

827 **Fig. 4:** The proxisome of TbPH1. **(A)** IFA showing localisation of TbPH1-BioID2-HA. Cells were labelled
828 with anti-HA (red) and DAPI. The scale bar corresponds to 5 µm. **(B)** IFA showing localisation of
829 biotinylated proteins. Cells were labelled with streptavidin-AF488 (green) and DAPI. The scale bar
830 corresponds to 5 µm. **(C)** Western blot (top panel) and stain-free gel (bottom panel) of a
831 representative BioID experiment. The blot was probed with anti-HA to confirm the presence of
832 TbPH1-BioID2-HA in the respective fractions. E: extract, SN: supernatant, F: flow through, B: boiled
833 beads. **(D)** Volcano plot with -10 log t-test p value plotted against the t-test difference between
834 TbPH1-BioID2-HA sample and mock (SmOxP9 cells) from three biological replicates. Statistically
835 significant hits are found above the curve in the top right quadrant and their identity is indicated.
836 Accession numbers are given with additional annotations in parentheses; these are color coded

837 based on their localization determined by TrypTag [37]. **(E)** Heat map of SAINTq score (*i.e.* P value) of
838 proteins interacting with TOEFAZ1 [28], positions of proteins also found in the TbPH1 proxisome are
839 indicated. a: Tb927.8.6830 (kinesin), b: Tb927.3.2490 (PH1), c: Tb927.8.1950 (ApbE-like domain), d:
840 Tb927.9.15470 (KifX2), e: Tb927.3.4720/60 (DLP1/2).

841 **Fig. 5:** TbKifX2 localises to the MtQ. **(A)** IFA on extracted cytoskeletons probing co-localisation of
842 TbKifX2-HA with an HA antibody. Cells were counterstained with anti-V5 to detect TbPH1-V5. **(B)** IFA
843 on extracted cytoskeletons probing co-localisation of TbKifX2-HA with the FAZ. Cells were
844 counterstained with L3B2 (recognising the FAZ filament, green). **(C)** IFA on extracted cytoskeletons
845 probing co-localisation of TbKifX2-HA with anti-HA antibody with basal bodies. Cells were
846 counterstained with YL1/2 (recognising mature basal bodies, green) **(D)** IFA on extracted
847 cytoskeletons probing co-localisation of TbKifX2-HA with the MtQ. Cells were counterstained with
848 mAB 1B41 (recognising the MtQ, green). The scale bar for all IFAs corresponds to 5 µm. **(E)**
849 Ultrastructure expansion microscopy of TbPH1 and TbKifX2. Cells were labelled with anti-V5/HA
850 antibody (purple) and anti-tubulin antibody C3B9 (grey) to visualize the MT corset. Punctate
851 cytosolic signals are visible in these preparations. **(F)** Ultrastructure expansion microscopy of TbPH1
852 and TbKifX2 (close-up view of posterior part of the cell). Cells were labelled with anti-V5/HA
853 antibody (purple) and anti-tubulin antibody C3B9 (grey) to visualize the MT corset. Purple arrows are
854 pointing to the MtQ signal.

855 **Fig. 6:** Depletion of TbPH1 and TbKifX2 causes multicellular aggregates and affects posterior end
856 remodelling. **(A)** Bar chart showing population doubling times for TbPH1, TbKifX2 and
857 TbPH1/TbKifX2 depletion cell lines. -/+: -/+ doxycycline to induce RNAi, the average difference in
858 hours from three experiments is shown above the respective bars. **(B)** Western blot of cellular
859 fractionation experiment following TbKifX2 RNAi. The blot was probed with anti-HA (to detect
860 TbKifX2), anti-V5 (to detect TbPH1) and anti-α-tubulin as a loading control. WCL: whole cell lysate.
861 **(C)** IFA of TbPH1/TbKifX2 RNAi cells. + tet: induced for 5 days. Extracted cytoskeletons were labelled

862 with L3B2 (recognising the FAZ filament, red), mAB 1B41 (recognising the MtQ, green) and DAPI. The
863 scale bar corresponds to 5 µm. **(D)** Phase contrast images of TbPH1/TbKifX2 RNAi cells. + tet:
864 induced for 5 days. The scale bar corresponds to 5 µm. Arrows indicate morphological defects.

865 **Fig. 7:** Scanning electron microscopy of TbPH1/TbKifX2 RNAi cells. Boxed images: uninduced cells.
866 Remaining images: cells 5 days post induction. Arrows pointing to posterior end protrusions. The
867 scale bar on the top left corresponds to 10 µm and is valid for all images except the one at the top
868 right in which the scale bar corresponds to 1 µm.

869 **Fig. 8:** Model depicting the potential role of the putative TbPH1/TbKifX2 heterocomplex. On left is a
870 close up of the heterocomplex. The ATPase activity of the N-terminal kinesin motor domain of
871 TbKifX2 likely drives movement to the plus end of the MtQ, while the PH domain is presumed to
872 carry a still unidentified cargo (X in yellow circle). Top right shows the heterocomplex in the context
873 of the *T. brucei* cell, depicting the more likely scenario that the heterodimer moves from the minus
874 ends of the MtQ MTs (red) between the mature and pro-basal bodies (pink) to their plus ends at the
875 anterior of the cell body, carrying auxiliary factor X. Upon RNAi depletion of TbPH1 and TbKifX2, this
876 factor accumulates at the posterior end, promoting extrusion formation.

877 **S1 Fig.:** Schematic depiction of 'microtubule sieving' technique. According to [32].

878 **S2 Fig.:** Schematic depiction of proximity-dependent biotinylation (BioID). According to [40]. Only
879 steps in black were performed in our study.

880 **S3 Fig.:** Ultrastructure expansion microscopy of a cell labelled with anti-ClpGM6 (to detect the FAZ,
881 purple) and anti-tubulin antibody C3B9 (grey) to visualize the MT corset.

882 **S4 Fig.:** TbPH1/TbKifX2 RNAi. **(A)** Growth curves of TbPH1 and TbKIfX2 RNAi cell lines. Filled circles:
883 TbKifX2 – tet, open circles: TbKIfX2 + tet, filled triangles: TbPH1 – tet, open triangles: TbPH1 + tet.
884 Insets show western blots probed with anti-HA (to detect TbKifX2), anti-V5 (to detect TbPH1) and
885 anti-α-tubulin as a loading control. **(B)** Growth curve of TbPH1/TbKifX2 RNAi cell line. Filled circles:

886 TbPH1/TbKifX2 – tet, open circles: TbPH1/TbKifX2 + tet. **(C)** Western blot showing depletion of
887 TbPH1/TbKifX2. Samples were taken at the same time as the growth curve in B was performed. The
888 blot was probed with anti-HA (to detect TbKifX2), anti-V5 (to detect TbPH1) and anti-α-tubulin as a
889 loading control. **(D)** Bar chart depicting different cell cycle phases during TbPH1/TbKifX2 RNAi time
890 course. DAPI counts were performed in triplicate with at least 200 cells counted per time point. N:
891 nucleus, K: kinetoplast.

892 **S5 Fig.:** Transmission electron microscopy and IFA of TbPH1/TbKifX2 RNAi cell line. Cells were
893 induced for 5 days. **(A)** Image depicting posterior end protrusions (arrow). The scale bar corresponds
894 to 1 µm. **(B)** Flagellar pocket region of cells not induced for TbPH1/TbKifX2. The scale bar
895 corresponds to 500 nm. **(C)** Flagellar pocket region of cells induced for TbPH1/TbKifX2 RNAi. The
896 scale bar corresponds to 500 nm. **(D)** IFA on cytoskeletons probing effects of TbPH1/TbKifX2
897 depletion post-translational modifications of tubulin. Cells were counterstained with GT335 (red,
898 staining glutamyl side chains) and YL1/2 (green, staining tyrosinated α-tubulin). The scale bar
899 corresponds to 5 µm. **(E)** Western blots taken after 3 to 5 days (d) of growth in presence (+) or
900 absence (-) of doxycycline probed with antibodies recognizing GT335, YL1/2 and α-tubulin, the last
901 as a loading control.

902 **S1 Dataset:** Mass spectrometry analysis of excised bands B1 and B2 from Fig. 3B.

903 **S2 Dataset:** Mass spectrometry data of TbPH1 BioID experiment. Data with and without imputation
904 and filtered for Andromeda scores >20 and presence of >1 peptide, which was used to
905 generate the volcano plot in Fig. 4D.

Fig. 1

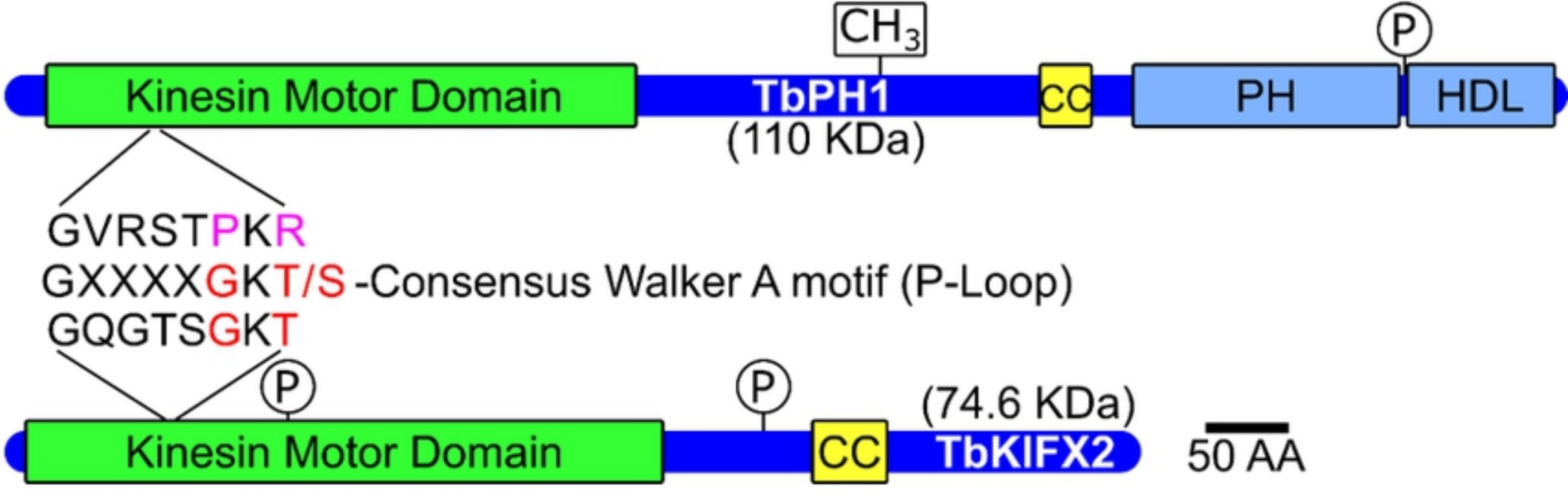

Figure 1

Fig. 2

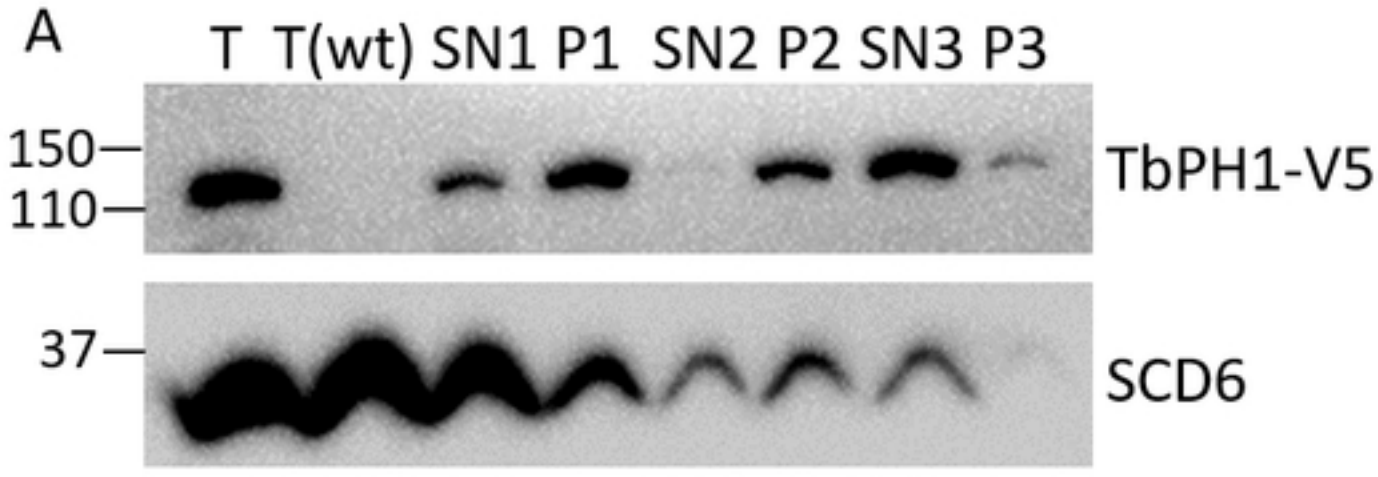

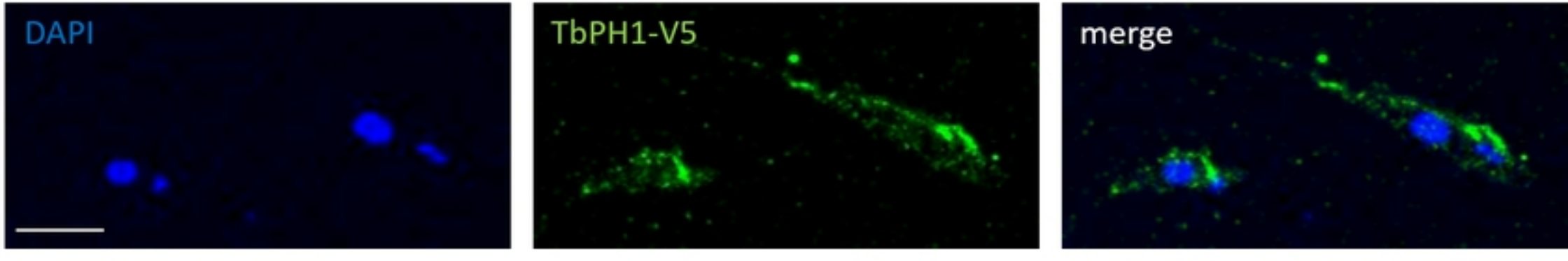

Figure 2

Fig. 3

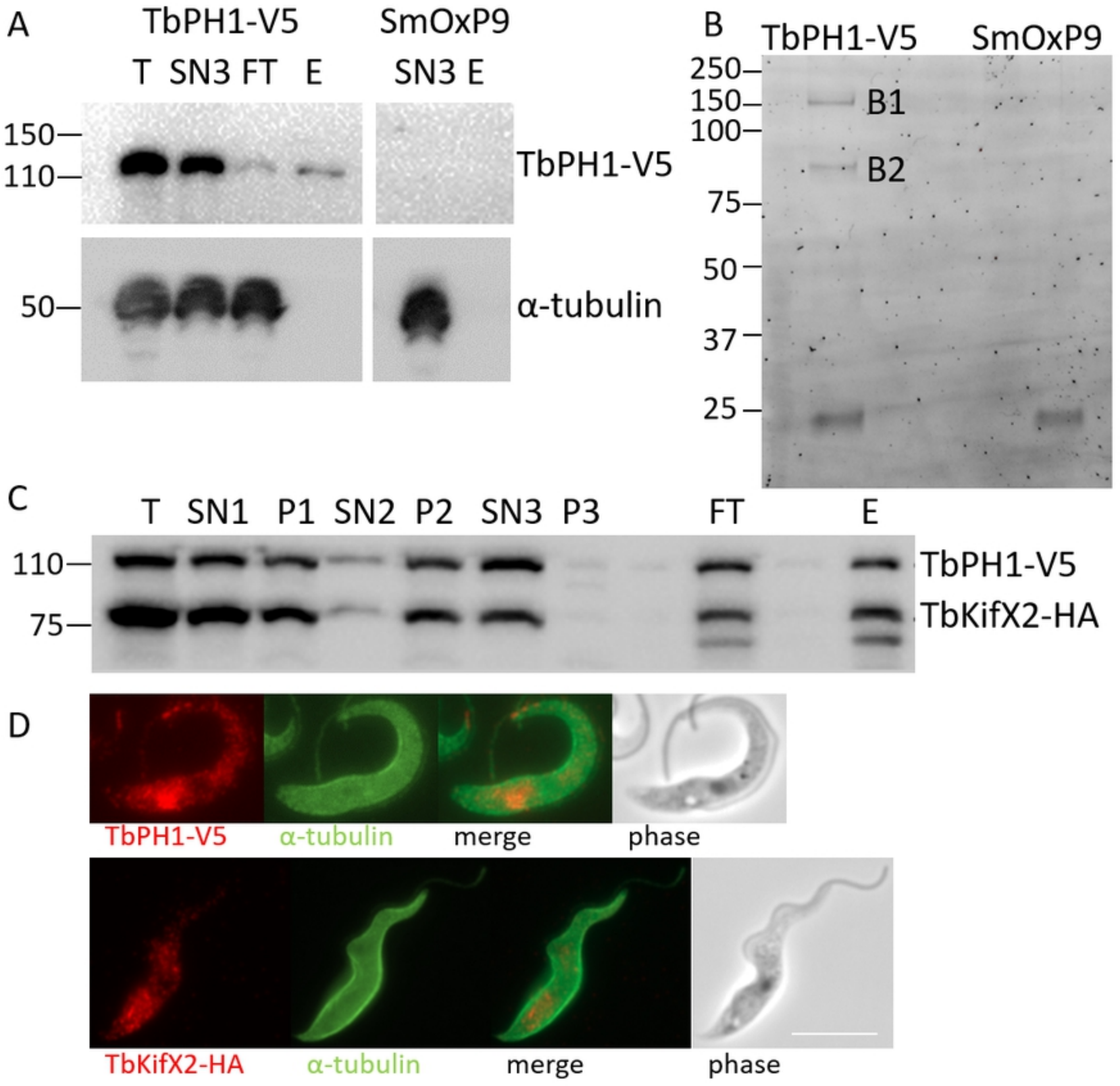

Figure 3

Fig. 4

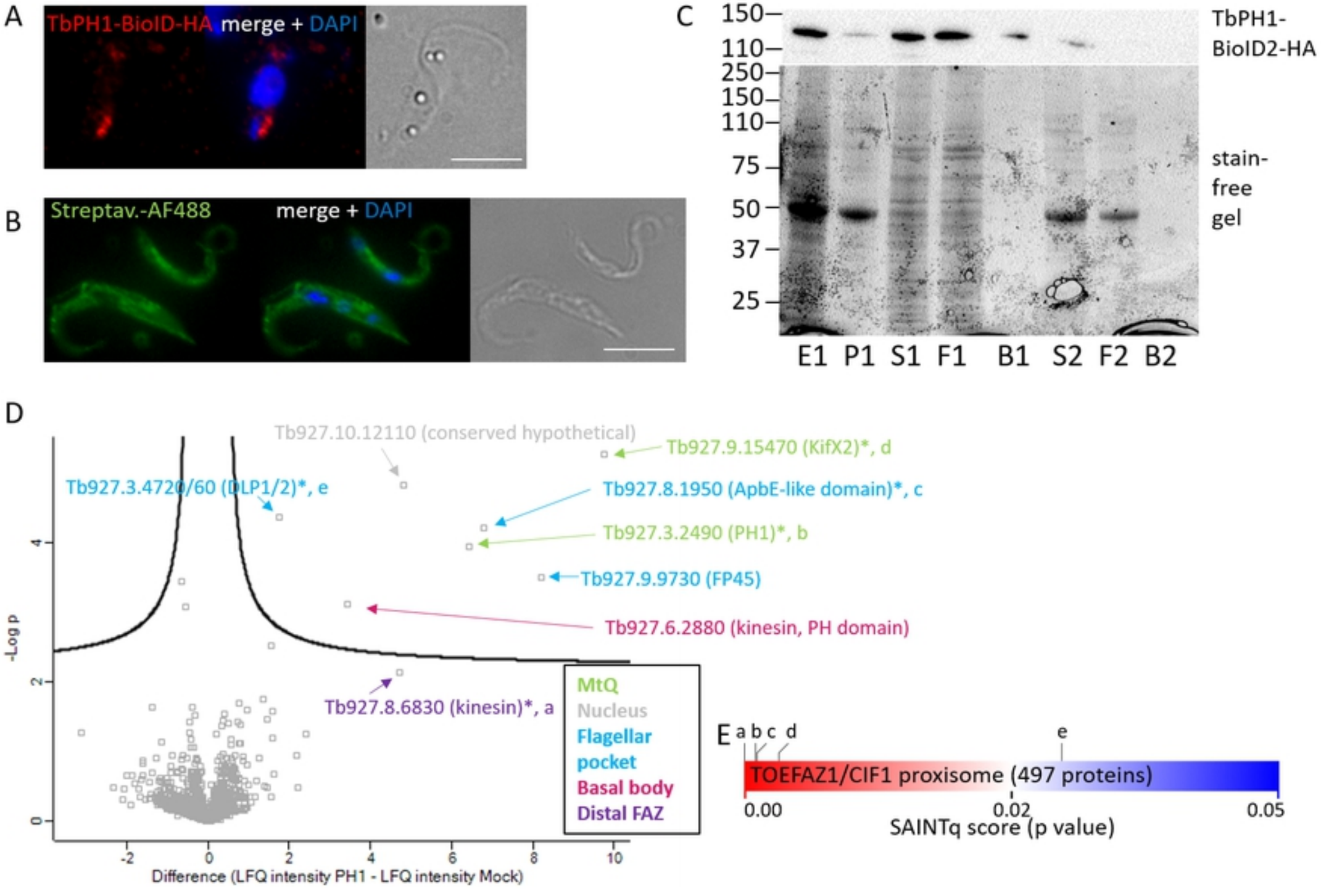

Figure 4

Fig. 5

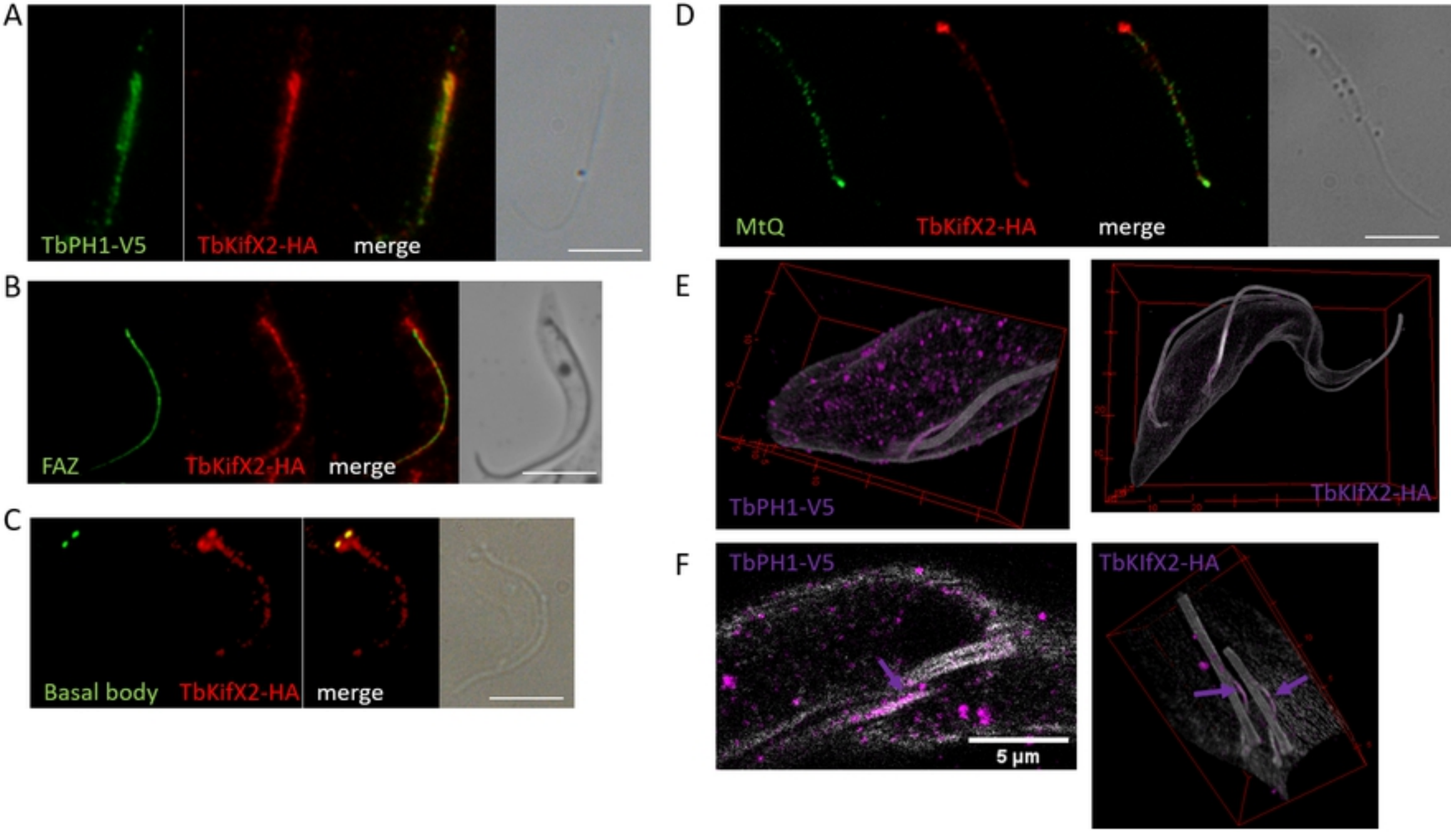

Figure 5

Fig. 6

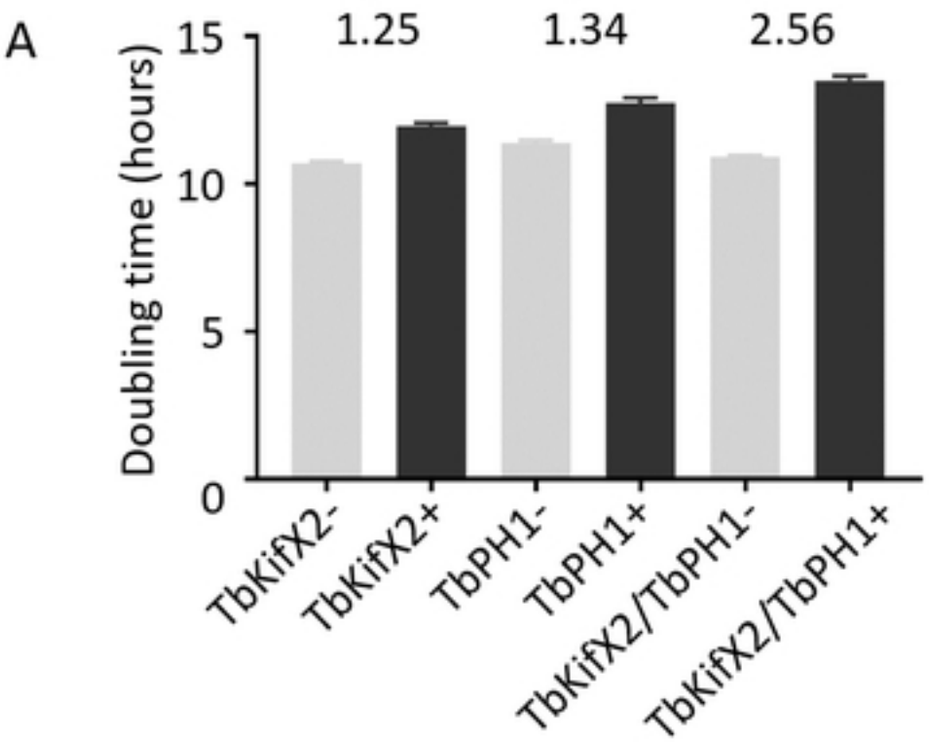

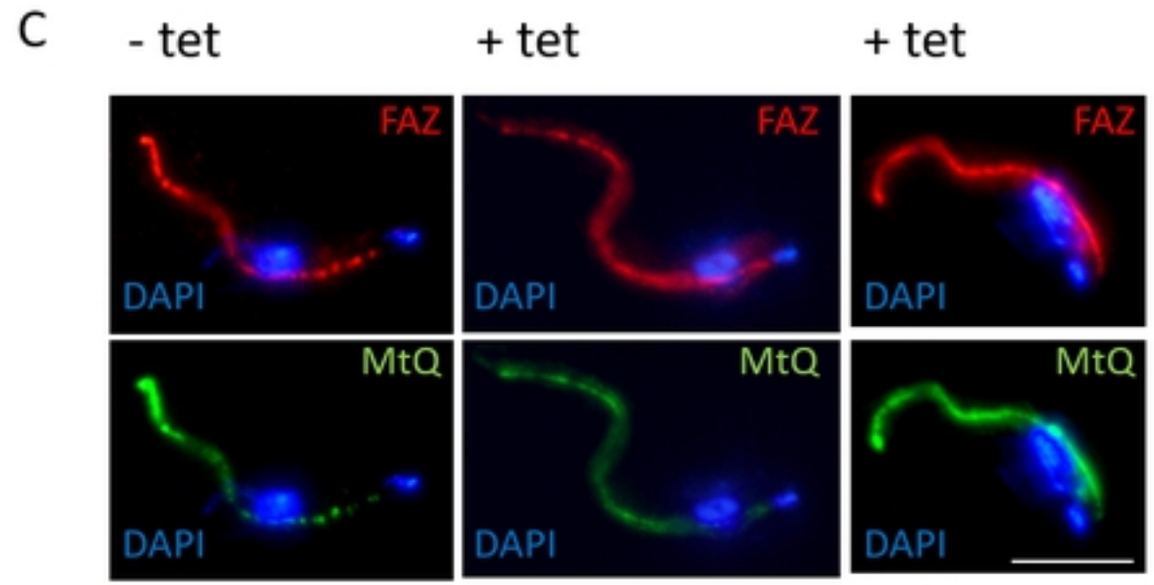

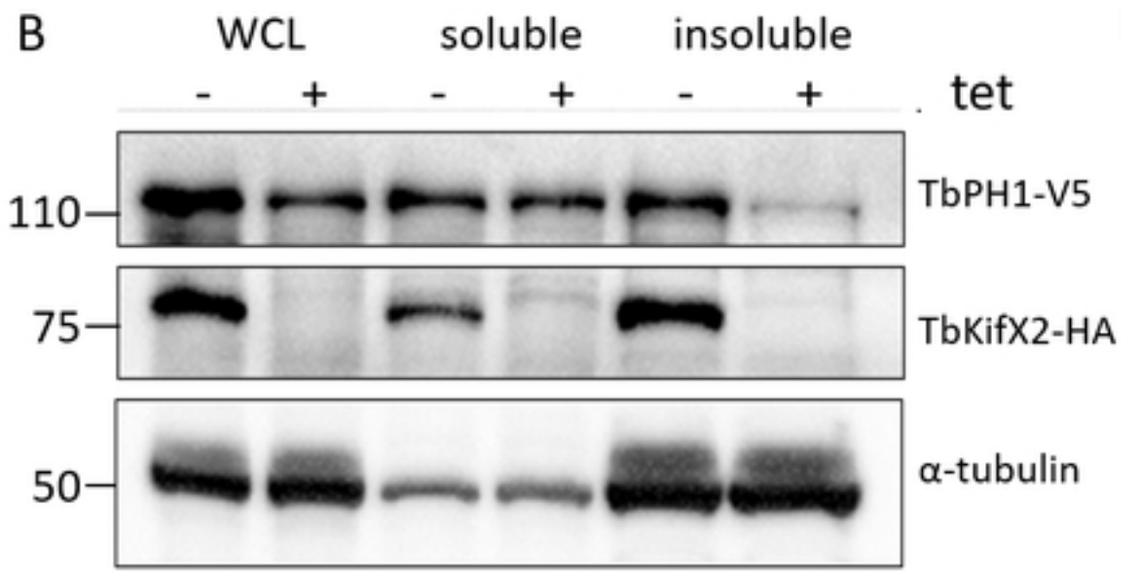

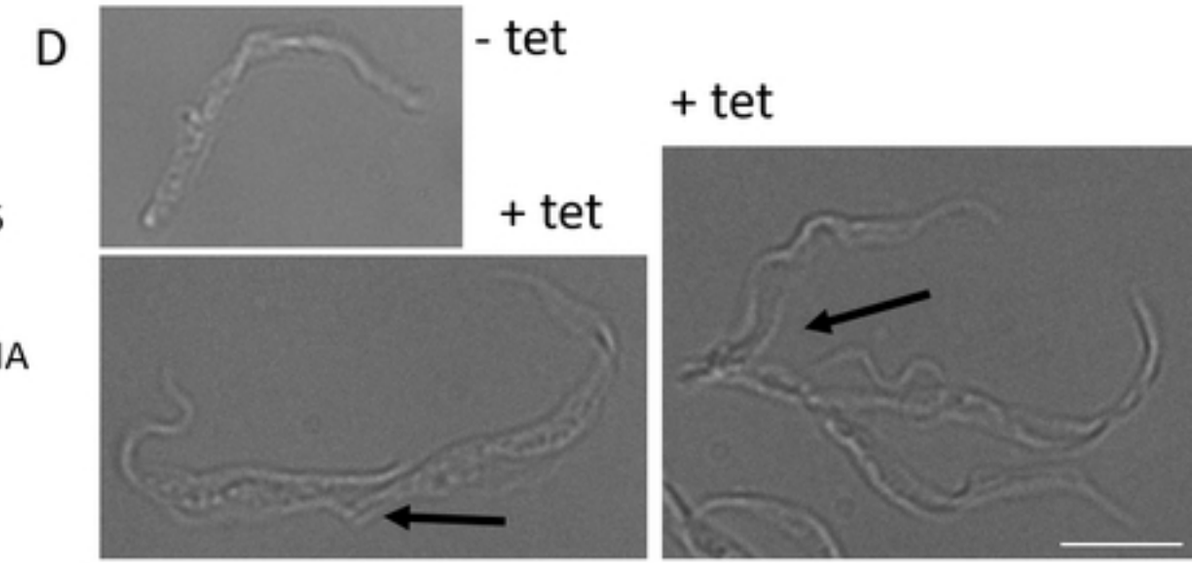

Figure 6

Fig. 7

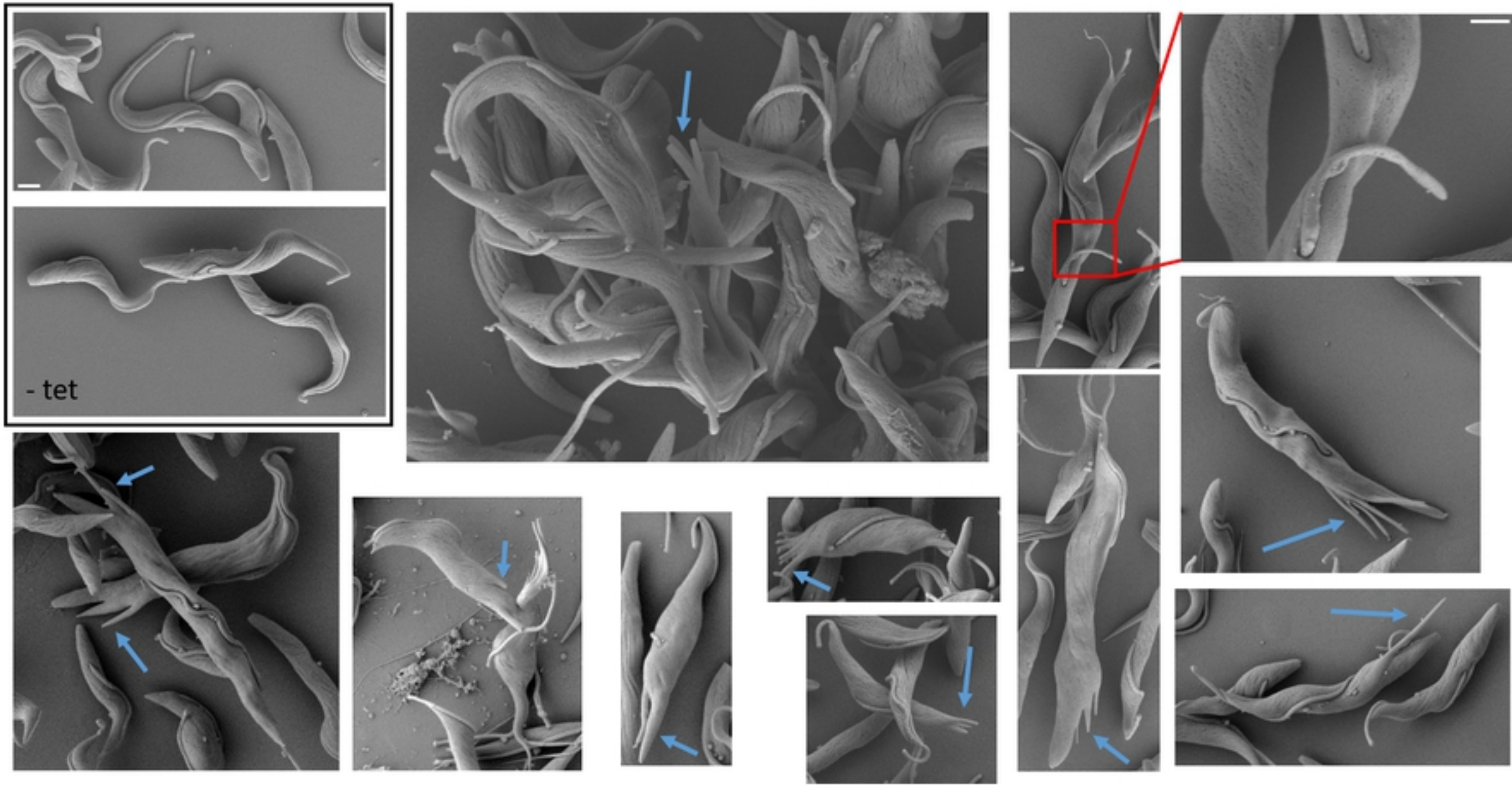

Figure 7

Fig. 8

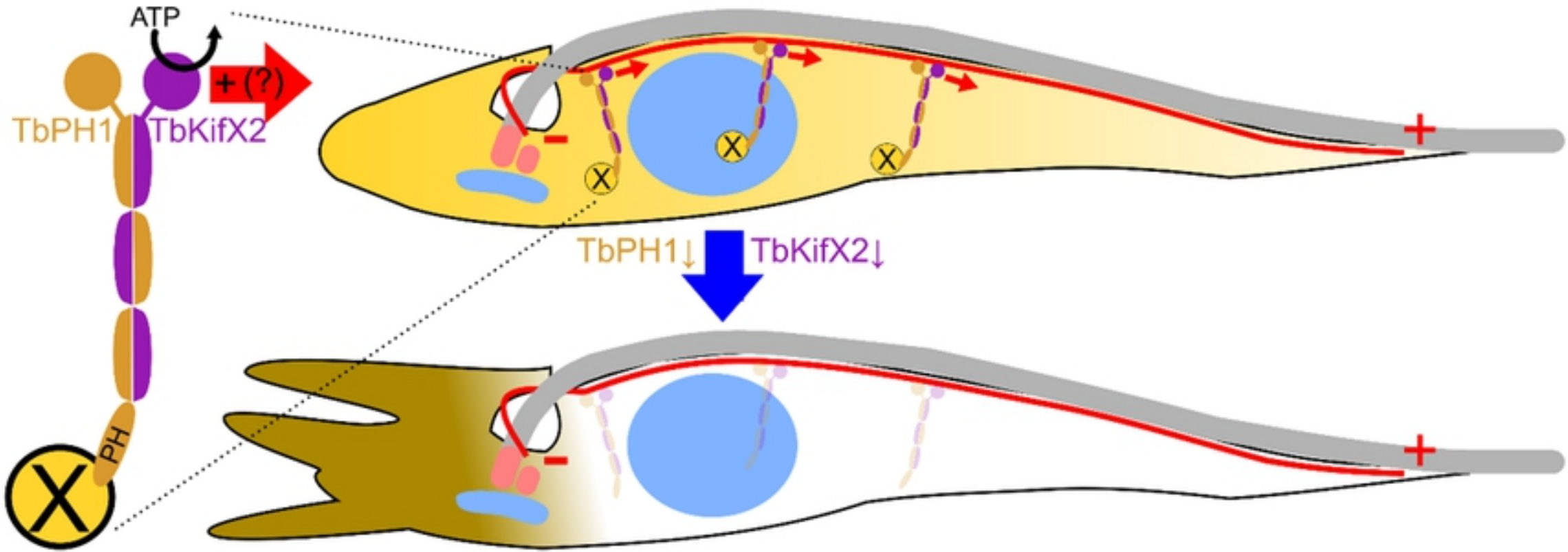

Figure 8